iberiancomsolconference.com

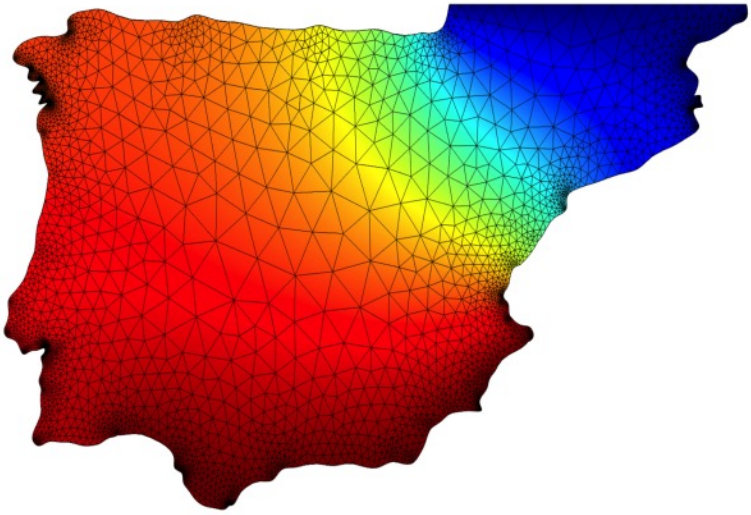

Iberian COMSOL Multiphysics CONFERENCE

Málaga. June 11, 2015

Organised by:

COMSOL

Uma Universidad de Málaga

NAFEMS

Addlink Software Científico

In collaboration with:

Andalucía Tech

FGUMA Fundación General Universidad de Málaga

EPS Escuela Politécnica Superior Universidad de Málaga

scbi uma

Sponsored by:

Addlink Software Científico

Iberian
COMSOL Multiphysics
Conference 2015
Málaga, June 11, 2015

Conference book, abstracts and papers

ISBN 978-84-608-5645-0

Contents

Welcome to Iberian COMSOL Multiphysics Conference 2015 in Málaga!

It is with great pleasure that we welcome you in Málaga to participate in the Iberian COMSOL Multiphysics Conference 2015.

In the conference we have tried to bring together a community that is scientifically diverse in an event that allows for inspiring contacts about the use of COMSOL Multiphysics, with the creation of a premier Iberian event for Multiphysics Modelling & Simulation. It is an event to connect with the Spanish and Portuguese COMSOL Multiphysics users and participate in training opportunities and events explicitly designed for the academic and engineering community. Oral and poster presentations highlight achievements in multiphysics modelling and simulations using COMSOL.

In addition to being inspired by new methods, ideas and knowledge, we hope you will also discover and enjoy the city of Málaga. Very ancient Phoenician and Punic archaeological sites have been found in Málaga. It was a Roman municipality and during the Moorish era became the capital of a small independent kingdom. Since the 1960s, it has been an international tourist destination and the centre of one of the most thriving regions in southern Spain. Málaga is a city for all tastes with activities for everyone, and a perfect city for shopping while exploring the downtown core. With more than twenty museums, fifteen of them concentrated in the same area, Malaga has truly become a City of Museums. In the historic downtown core alone, including the new projects that will come on stream shortly, there are up to 24 museums making Malaga's historic downtown core one of the most densely developed in terms of museums.

Finally, we would like to thank Addlink Software Científico, COMSOL AB, the Technical Secretariat of the FGUMA, the University of Málaga, the Scientific Committee and the invited lectures for their assistance, and all the helping hands whose efforts will undoubtedly make Iberian COMSOL Multiphysics Conference 2015 a conference to remember!

The organizing committee of Iberian COMSOL Multiphysics Conference 2015.

Conference program

June 11, 2015

Morning	
9:00	**Registration Opens**
9:30 - 9:45	**Welcome and Introduction**
9:45 - 10:15	**Keynote presentation.- Creating and Running Multiphysics Apps.** Ed Fontes. *COMSOL AB, Sweden.*
10:15 - 10:45	**User's presentations.** Session 1.
10:45 - 11:15	*Coffee Break*
11:15 - 12:15	**Minicourse.- Application Builder and COMSOL Server.** Ed Fontes. *COMSOL AB, Sweden.*
12:15 - 12:45	**User's presentations.** Session 2.
12:45 – 13:15	**Keynote presentation.- Electromagnetic Field Simulation in Microwave Ovens: from code to COMSOL Multiphysics.** João Pedro Sousa. *Teka Portugal S.A., Portugal*
13:15 - 14:30	*Lunch*

Afternoon	
14:30 - 15:30	**Minicourse.- Solving industrial design problems by using COMSOL Multiphysics with MATLAB.** Benjamín Ivorra. *Complutense University of Madrid, Spain.*
15:30 - 16:15	**User's presentations.** Session 3.
16:15 - 16:45	**Poster session.**
16:45 - 17:15	**Keynote presentation.- Geometry induced biofilm formation.** Ana María Carpio Rodríguez. *Complutense University of Madrid, Spain.*
17:15	*Conference Ends*
20:30	*Conference Cocktail*

10:15 – 10:45 **User's presentations.** Session 1.

10:15 - 10:30 Electrical-thermal Coupled Physics with COMSOL Multiphysics to Model Thermal Ablation of Tumors. M. Trujillo and E. Berjano.

10:30 - 10:45 Piezoelectric Sensor Design with Metal Shield, J. Barreiro, A. Sáenz de Inestrillas and F. Camarena.

12:15 – 12:30 **User's presentations.** Session 2.

12:15 - 12:30 Influence of Overhead Power Conductor Shape on its Temperature, J. C. del-Pino-López, D. Garrido-García, P. Cruz-Romero and A. Gómez-Expósito.

12:30 - 12:45 Modelling Interfacial Shear Stresses in Electrohydrodynamics with COMSOL, P. García-Sánchez.

15:30 – 16:15 **User's presentations.** Session 3.

15:30 - 15:45 Interfacing Multiphysics and Geochemistry in Porous Media, E. Abarca, A. Sainz, D. Sampietro, O. Silva, A. Idiart, J. Molinero.

15:45 - 16:00 Analysis and Simulation of Thermal Energy Mechanism and Convection Processes in the Halls and Courtyards of the Alhambra in Granada, D. Blasco-Avellaneda, A. Martínez and D. Ruiz.

16:00 - 16:15 Copper Slag-Matte Decantation Studies, C. Bontoiu, I. Moreno-Ventas, M. Bacedoni and F. J. Blas.

16:15 – 16:45 **Poster session.**

P1: Ultrasonic Drying Design: Acoustic-Structure Interaction Modeling, J. Bon, V. Acosta, E. Riera and A. Pinto.

P2: Acoustic Studies of Bubble Chamber for Direct Dark Matter Searches, I. Felis and M. Ardid.

P3: Copper Slag-Matte Decantation Studies, C. Bontoiu, I. Moreno-Ventas, M. Bacedoni and F. J. Blas.

P4: Microfluidic Cell Trapping Device for Single-Cell Studies, C. Freitas, C. Mendes, F. Pereira, E. Fortunato, R. Martins, H. Águas and A. Oliva.

P5: Three-Dimensional Modeling of Scanning Microwave Microscopy Applied to a Single Bacterial Cell, R. Fabregas, M. C. Biagi, L. Fumagalli and G. Gomila.

P6: Numerical Simulation of Piezoceramic Elements, J. Barreiro, A. Saenz de Inestrillas and F. Camarena.

Keynote presentations and minicourse

Invited speakers

Ed Fontes.
COMSOL AB, Sweden

Ph.D. in Electrochemical Engineering from the Royal Institute of Technology in Stockholm. Ed Fontes is Chief Technology Officer at COMSOL. He is part of the group that decides the content and plans the work for developing COMSOL Multiphysics, its add-on products, and COMSOL Sever. He is also deeply involved in the specification and implementation of the electrochemical engineering functionality in COMSOL.

Keynote presentation.- Creating and Running Multiphysics Apps

Minicourse.- Application Builder and COMSOL Server

Abstract

The Application Builder allows users of COMSOL Multiphysics® to create their own graphical user interfaces (GUI), for specific purposes, to control an embedded multiphysics model. These tailored user interfaces, including the embedded model, are called applications or "apps". The purpose of creating these apps is to make it possible for engineers and scientists, that are not modeling experts, to benefit from multiphysics modeling and simulations for their specific needs. As a COMSOL Multiphysics user, you may develop apps for students, friends, colleagues, partners, and customers. You can also charge your customers for the apps.

COMSOL Server is able to host the server processes that drive the apps with the user interface run on a local client, for example an html-client or a desktop client. The combination of the Application Builder and COMSOL Server™ makes it very straight forward for modeling experts to develop and share their apps.

This presentation and minicourse demonstrate the use of the Application Builder for developing apps. It shows how you can graphically design user interfaces by dragging and dropping graphic forms and widgets such as menus, input fields, buttons, checkboxes, plot figures, etc. Also the linking of graphics

widgets to commands that control the embedded model is demonstrated: for example to control model parameters, mesh, solvers, and results. A demo of the use of COMSOL Server to administrate and run apps gives you a glimpse of the possibilities with this new functionality.

Benjamín Ivorra
Complutense University of Madrid, Spain

Ph.D. in Applied Mathematics at the University of Montpellier (France). His main research themes are about optimisation methods and their applications to industrial problems. In particular, he has extensively used COMSOL Multiphysics to model and solve design problems, such as improvement of microfluidic mixers, study of the effect of Pressure/Temperature in food treatment devices or conception of Pulsed Electric Field chambers.

Minicourse.- Solving industrial design problems by using COMSOL Multiphysics with MATLAB

Abstract

COMSOL Multiphysics is a very efficient tool for modeling numerically complex devices. In particular, this software can be used during the industrial design processes involving optimization problems. One interesting characteristic of COMSOL Multiphysics is the possibility of incorporating the created model into a MATLAB script code. This allows the MATLAB script to automatically change some considered model parameters, such as geometrical shapes, physical characteristics, etc. Thus, any optimization algorithm compatible with MATLAB script can solve an optimization problem involving a COMSOL Multiphysics model. During this minicourse, first we will detail the basic steps to create and solve industrial design problems by coupling COMSOL Multiphysics with MATLAB. Then, we will illustrate the presented methodology by considering the optimization of a fast hydrodynamic focusing microfluidic mixer for protein folding.

João Pedro Sousa
Teka Portugal S.A., Portugal

Licentiate in Physics Engineering by the University of Aveiro, Portugal. He is Senior R&D Engineer in the Research & Development Department at Teka Portugal S.A. Integrator of COMSOL Multiphysics on microwave ovens research and design. Technical and Scientific Consultant to the GREENWAVE and CURECORK projects (EU funded projects) on computer simulations with COMSOL Multiphysics of electromagnetic fields and heat generation/transfer on ceramics composites and cork agglomerates. He also maintain a strong collaboration with the Physics Department of the University of Aveiro on microwave energy research.

Keynote presentation.- Electromagnetic Field Simulation in Microwave Ovens: from code to COMSOL Multiphysics

Abstract

In a short sentence, designing a microwave oven involves mastering methods that allow the best energy transfer, the maximum energy containment and an optimal load thermal energy distribution. From an experimental point of view these three components have to be dealt with an equal importance in order to achieve the best equilibrium possible. Spite the reliability of such methods they have the drawback of being time consuming, any variant in design requires a full set of analysis to be validated. Computer simulations, using the FTDT method coded in FORTRAN, were first used to compare results of simulated radiation leakage of several designs of a microwave oven´s doors against experimental measurements. Simulation and experimental data matched perfectly, and with this the confidence in simulation methods increased. COMSOL Multiphysics was first used in GREENWAVE, a project intended to create industrial hybrid microwave/gas ovens, to simulate the electromagnetic field distribution inside and subsequent heating pattern on ceramic composites. This originated three prototypes with microwave output powers ranging from 6 kW to 20 kW. In the following project, CURECORK, a small prototype of 2 kW was created to evaluate the feasibility of microwave energy in the thermal curing process of cork agglomerates under higher pressures. In 2014 Teka

Portugal S.A. acquired a COMSOL Multiphysics license to begin simulations on EM fields in microwave ovens, load's heating pattern and leakage through the oven´s door. Although this research is at an early beginning, the primary results rouse an interest in the use of COMSOL Multiphysics in CFDs, intended to simulate oven's cooling systems and, more important, cooker hoods air flow pattern in order to achieve better products in terms of fluid dynamic efficiency.

Ana María Carpio Rodríguez.
Complutense University of Madrid, Spain.

Professor of Applied Mathematics in the Universidad Complutense de Madrid. She received her Ph.D. degree from the Laboratoire d'Analyse Numérique (now Jacques Louis Lions, Université Paris VI, 1993) and conducted her postdoctoral research in the Oxford Centre for Industrial and Applied Mathematics (University of Oxford, 1996–1997). Her research interests span upon a wide variety of problems, ranging from applied topics, such as multiscale modeling of bio- and nano-systems, imaging, or the study of defects in graphene, to theoretical and numerical analyses of differential equations. Her recent work on the formation and spread of biofilms in medical and industrial flow systems has made extensive use of COMSOL Multiphysics.

Keynote presentation.- Geometry induced biofilm formation

Abstract

Bacteria in aqueous environments usually gather to form aggregates called biofilms. In biofilms, cells display many behavioural differences from planktonic cells, such as a 1,000-fold increase in tolerance to antibiotics. Hospital-acquired infections are often caused by biofilm spread through medical systems. Design improvements hindering biofilm formation rely on identifying factors that favour their appearance. We will see that the presence of corners and narrowings in medical flow circuits triggers biofilm nucleation by creating secondary vortical motion driving bacteria to walls. Detailed flow studies in micro- and mili-fluidic devices support that observation. Once biofilm seeds are

created, they proliferate forming filaments whose structure is again controlled by the geometry. In this work, COMSOL Multiphysics has been extensively used to identify flow structures induced by the geometry that affect the biofilm formation process.

Abstracts Oral presentations

Electrical-thermal Coupled Physics with COMSOL Multiphysics to Model Thermal Ablation of Tumors

M. Trujillo[*1], E. Berjano[2]

[1]Instituto Universitario de Matemática Pura y Aplicada. Universitat Politècnica de València,
[2]Biomedical Synergy, Electronic Engineering Department, Universitat Politècnica de València.
*Departamento de Matemática Aplicada. Escuela de Arquitectura. Universidad Politécnica de Valencia. Camino de Vera s/n. 46022. Valencia. Spain, matrugui@mat.upv.es

Abstract

Radiofrequency ablation (RFA) is a minimally invasive thermal therapy aimed to destroy malignant tissue, usually cancer (see for example [1] and [2]). Electrical currents are applied in the tissue through a metallic electrode, and produce heating in the tissue due to ionic friction. When tissue temperature is over 50ºC for several minutes an irreversible thermal lesion is produced. All the damaged tissue constitutes the called coagulation zone. A lot of research effort has been done to enlarge the coagulation zone, which would guarantee the complete destruction of large tumors. Experimental studies have demonstrated that using a pulsed protocol of electrical power delivering (also called constant impedance protocol) allows creating larger coagulation zones compared to a continuous protocol [3]. It consists on alternating higher peak current with low current deposition.

From a theoretical point of view, there is no a solid explanation for this advantage. Numerical modeling is a cheaper and quick method to answer these issues. For these reasons, our aim was to build a confident model which can explain the tissue electrical and thermal behavior during a pulsed RFA.

The model was solved using COMSOL Multiphysics. We used a multiphysics problem which included the electrical and thermal problem and a general PDE coefficient form problem to compute the coagulation zone. All computer simulations were performed with a Dell T7500 workstation with Six Core, 2.66 GHz Xeon processors and 48 GB RAM running on a Windows 7 Professional 64 bit operating system.

Results for computer simulations were compared to previous experimental results to validate the theoretical model.

Future results could assist in improving the performance and safety of pulsed protocols in RFA by suggesting other protocols to create larger lesions in a more predictable way.

References

1. Sharma R, Wagner JL, Hwang RF, Ablative therapies of the breast, *Surg Oncol Clin N Am*, **20**, 317-39 (2011).

2. Savoie PH, Lopez L, Simonin O, Loubat M, Bladou F, Serment G *et al*, Two-years follow-up of radiofrequency thermotherapy for urination disorders due to benign prostatic hyperplasia, *Prog Urol*, **19**, 501–6 (2009).
3. Goldberg SN, Stein MC, Gazelle G S, Sheiman RG, Kruskal JB and Clouse ME, Percutaneous radiofrequecy tissue ablation: Optimization of pulsed RF tecnique to increase coagulation necrosis, *J Vasc Interv Radiol*, **10**, 907-16 (1999).

Piezoelectric Sensor Design with Metal Shield

J. Barreiro[1], A. Sáenz de Inestrillas [1], F. Camarena[1]

[1]Universitat Politècnica de València. Institut d'Investigació per a la Gestió Integrada de les Zones Costaneres.
* EPSG. C/Paranim 1, 46730 Grau de Gandia. fcamarena@fis.upv.es

Abstract

In industrial applications where sound pressure levels need to be registered in volatile chemical environments it is interesting to use waterproof and electromagnetically encapsulated sensors with great sensitivity. This requirement can be overcome by using very thin piezoelectric ceramics coupled with thin metal plates, where mechanical resonance of this last component, due to its physical properties of stiffness and elasticity, excite the ceramic, who will be responsible for transforming the mechanical movement into an electrical response.

COMSOL Multiphysics is used with the integrated solid mechanics to make a study of natural frequencies (Figure 1) and to determine the optimal radii and thicknesses in which the plate, the ceramic and transducer body resonates. There exist a theoretical approach to the problem based on the equations describing the vibration of plates (Figure 2) [1], but a more detailed study is needed to consider the complex geometry of the sensor.

The sensitivity of different approaches of the transducer has been calculated with COMSOL by using the piezo-acoustic module with a pressure condition as an input parameter (Figure 3) [2]. So that the simulation is able to determine the resulting voltage obtained when an acoustic wave excites the transducer at a particular frequency (Figure 4).

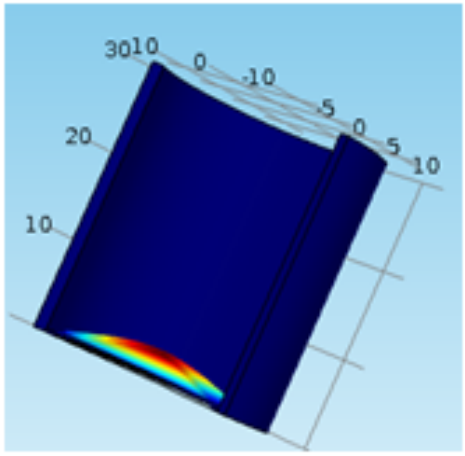

Figure 1. *Fundamental mode vibration. It has been considered the plate, the ceramic and the body of the transducer.*

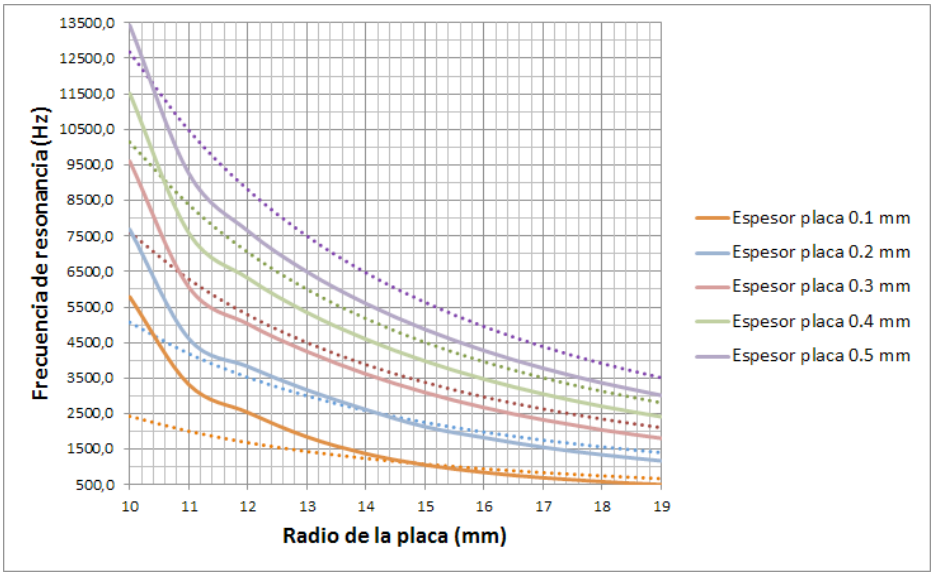

Figure 2.*Resonace frequencies of an aluminum plate with different radii and thickness. Ceramic radii 10 mm and thickness 0.3 mm. Dotted lines show the results obtained from the theoretical approach.*

Experimental results approximate simulation, considering that during manufacture of the sensor, which does not provide an automated process, it is not possible to control variables that lead to a mismatch model, as the amount of welding electrodes and epoxy driver when attaching and ceramic plate, which would be contemplated as an additional mass, compared to the thicknesses and sizes and ceramic plate. But in the end it can be seen that there is a relationship between thicknesses and material properties radios when adjusting a transducer like this. Finally, we provide a discussion about the effect in the sensitivity of the different parameters and coefficients of mechanical and electrical losses, something important is discussed when working with ceramics that are outside the database software materials.

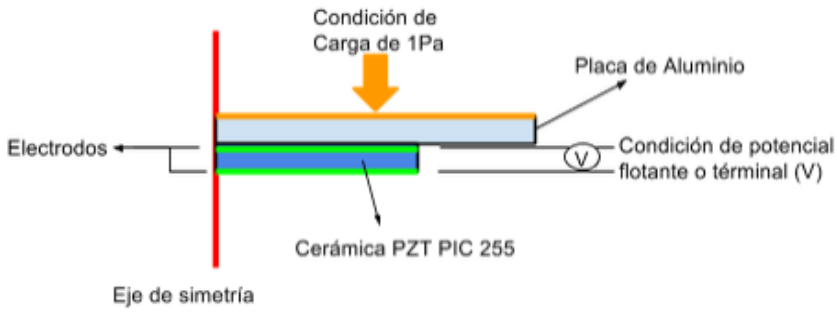

Figure 3. *Tranducer diagram for the sensitivity simulation. Piezoelectric module.*

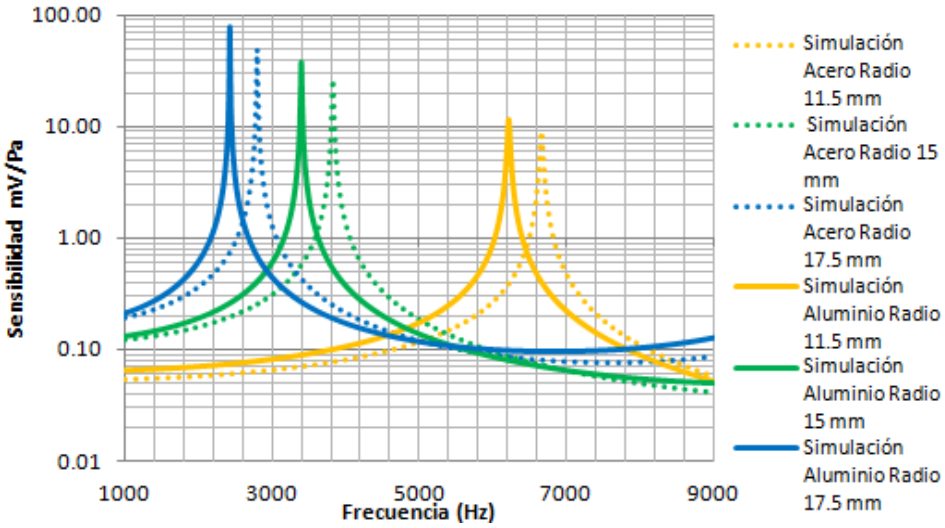

Figure 4. *Transducer sensitivity for different dimensions and materials.*

References

1. Kinsler, Lawrence E et al. "Fundamentals of acoustics." *Fundamentals of Acoustics, 4th Edition, by Lawrence E. Kinsler, Austin R. Frey, Alan B. Coppens, James V. Sanders, pp. 560. ISBN 0-471-84789-5. Wiley-VCH, December 1999.* 1 (1999).

2. Lerch, Reinhard. "Simulation of piezoelectric devices by two-and three-dimensional finite elements." *Ultrasonics, Ferroelectrics, and Frequency Control, IEEE Transactions on* 37.3 (1990): 233-247.

Influence of Overhead Power Conductor Shape on its Temperature

J. C. del-Pino-López*, D. Garrido-García, P. Cruz-Romero, A. Gómez-Expósito

Departamento de Ingeniería Eléctrica, Escuela Técnica Superior de Ingeniería, Universidad de Sevilla, Spain.
*Camino de los descubrimientos s/n, 41092, Sevilla, vaisat@us.es

Abstract

Due to the increase on electricity demand, the deregulation that imposes regulated revenues to transmission and distribution utilities, and the difficulty to build new overhead lines, in the last decades these lines are being operated close to their thermal limit, jeopardizing the security of the system. Therefore, it is of interest to study more efficient designs of power lines with the main goal of obtaining power conductor with higher current-carrying capacity (ampacity). In this sense, overhead power conductors are affected by different heat transfer mechanisms: solar heating, radiation, conductive and forced convection heat transfer. The latter is the main heat evacuation mechanism, and the amount of heat evacuated depends not only on the environmental conditions (wind direction, velocity and temperature), but also on the surface and shape of the conductor. Therefore, it is clear that a suitable shape for the conductor may reduce its maximum temperature, hence increasing its ampacity in comparison to standard round shape design.

The problem to be solved is rather complex, since there are three physics involved: an electromagnetic problem coupled to thermal and fluid dynamics ones. In this situation, the best choice is the use of a multiphysics software like COMSOL Multiphysics©. In this work, a complete finite element model is developed in COMSOL, where electromagnetic, thermal and fluid dynamics physics are fully coupled. In particular, three physics nodes are employed (Figure 1): Magnetic fields (*mf*), Heat transfer (*ht*), and k-ε turbulent flow.

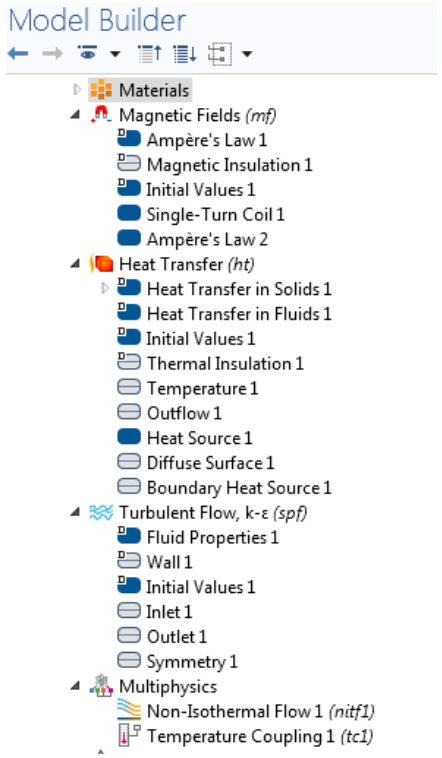

Figure 1. *Model nodes for the implementation of the multiphysics problem.*

The geometry of the conductor is modeled by means of two concentric layers, the external one made of aluminum and the internal one made of steel. Its shape is deformed in order to obtain different elliptical shapes. This is done by means of a parameter called "shape factor" (*SF*), which ranges from 0.5 to 1.5, being equal to 1 when a circular shape is desired (Figure 2).

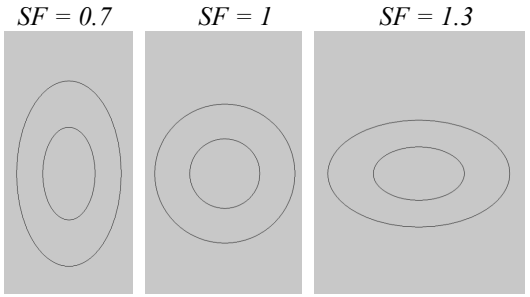

Figure 2. *Example of power conductor shapes for different SF values.*

The case of a 300 mm^2 power conductor is analyzed for a number of environmental and boundary conditions (wind direction, air velocity, ambient temperature, and current through the conductor) and different elliptical shapes. The COMSOL model provides

the results regarding the temperature and air velocity fields around the power conductor (Figure 3). In addition, a parametric analysis has been carried out in order to analyze the influence of the main geometrical and environmental parameters on the highest temperature achieved in the conductor (Figure 4).

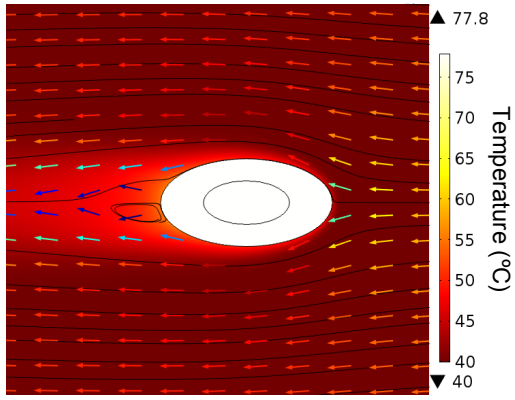

Figure 3. *Temperature and wind velocity field for SF = 1.4 (V_{in} = 1 m/s and I_0 = 750 A).*

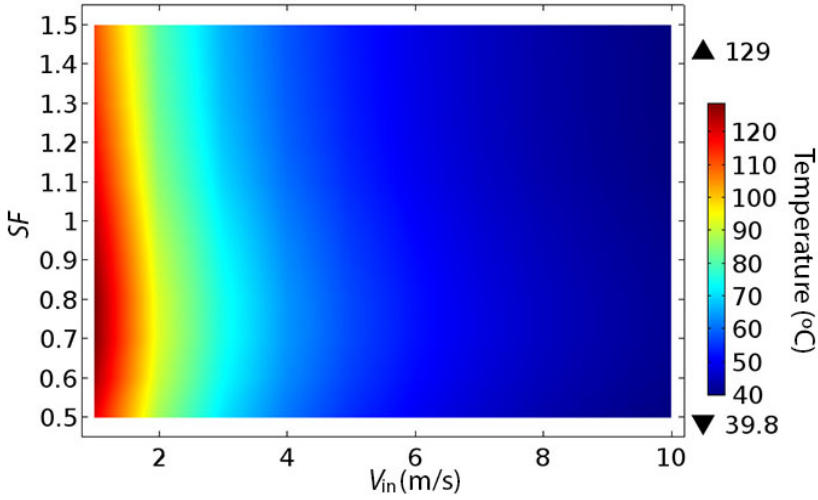

Figure 4. *Evolution of the maximum temperature with wind velocity and SF (I_0 = 1100 A and θ_{amb} = 20 ºC).*

From the results it is concluded that overhead power conductors may increase their current-carrying capacity if they have horizontal elliptical shape (*SF* > 1 in Figure 2) instead of a circular one. This increase may be in the range of 9 % depending on the environmental conditions. From this analysis it is also derived that the temperature of power conductors with elliptical shape is less sensitive to changes in the environmental conditions than the circular conductor, with the exception of the wind direction. This parameter influences negatively on the temperature of the elliptical conductor, but this is

only when the angle of incidence ranges from 0º to 30º (Figure 5). In the worst of these cases the temperature would achieve that of the circular conductor at most.

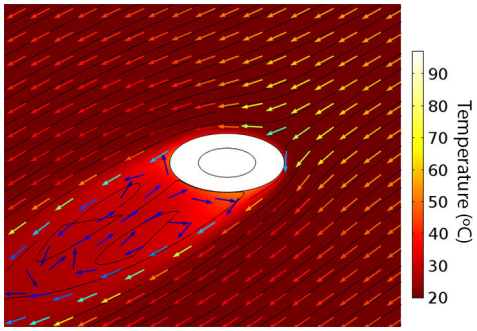

Figure 5. *Temperature and wind velocity field for SF = 1.4 and angle of incidence of 30º (V_{in} = 1 m/s, θ_{amb} = 20 ºC and I_0 = 900 A).*

References

1. CIGRÉ WG B2.43, Guide for Thermal Rating Calculation of Overhead Lines with high temperatures and real-time weather & load data, *Technical Report*, Draft 3.0 (2012).
2. L. Konti, A proposed algorithm for an overhead transmission line conductor temperature rise calculation, *International Transactions on Electrical Energy Systems*, **Volume 24**, page 578-596 (2014).
3. I. Makhkamova, *Numerical Investigations of the Thermal State of Overhead Lines and Underground Cables in Distribution Network*, Durham theses, Durham University (2011). Available at Durham E-Theses Online: http://etheses.dur.ac.uk/866/.
4. *COMSOL Multiphysics* Reference Manual, Version: October 2014 COMSOL 5.0.
5. *COMSOL* Heat Transfer Module User's Guide Version: October 2014 COMSOL 5.0.
6. *COMSOL* AC/DC Module User's Guide Version: October 2014 COMSOL 5.0.
7. *COMSOL* CFD Module User's Guide Version: October 2014 COMSOL 5.0.

Modelling Interfacial Shear Stresses in Electrohydrodynamics with COMSOL Multiphysics

Pablo García-Sánchez[*1]

[1]Depto. de Electrónica y Electromagnetismo. Universidad de Sevilla. Spain.
*Presenting and corresponding author: Avda Reina Mercedes S/N. Facultad de Física. 41014, Sevilla (Spain). pablogarcia@us.es.

Abstract

Many problems in Electrohydrodynamics are solved by finding the velocity in a liquid with boundaries subjected to shear stresses of electrical origin. If Reynolds number is small, it is possible to solve the velocity in the liquid with the use of the *Laminar flow* interface in COMSOL Multiphysics. However, it usually happens that we have to simultaneously impose a shear stress and zero normal velocity on a certain boundary and none of the predefined boundary conditions of the laminar flow interface allows for this possibility.

In this work we show how to impose zero normal velocity and a shear stress on boundaries by adding a weak contribution to the laminar flow interface. We solved a well-known problem in Electrohydrodynamics (Ref. 1) where the electrode configuration gives rise to a homogeneous shear stress and analytical solutions are available for comparison with the numerical results (Figure 1).

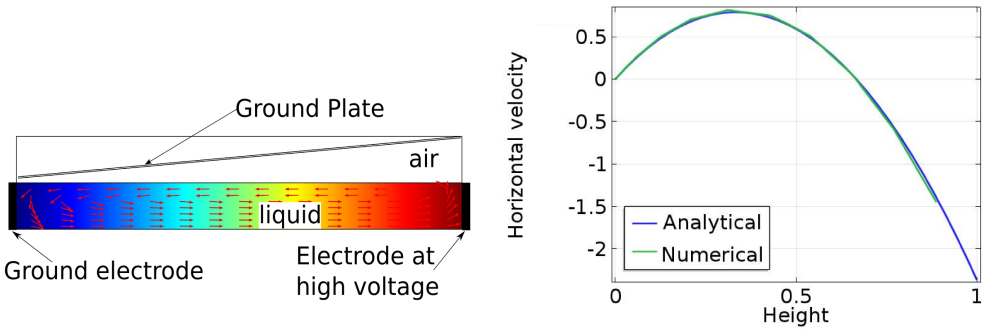

Figure 1: *(Left) Problem domain including electrodes. (Right) Comparison between analytical and numerical solutions for the horizontal liquid velocity.*

References

1. Melcher, J. R., & Taylor, G. I. (1969). Electrohydrodynamics: a review of the role of interfacial shear stresses. *Annual Review of Fluid Mechanics*, *1*(1), 111-146.

Interfacing Multiphysics and Geochemistry in Porous Media

Elena Abarca[1*], Alvaro Sainz[1], Diego Sampietro[1],
Orlando Silva[1], Andrés Idiart[1], Jorge Molinero[1]

[1] Amphos 21 Consulting, Passeig Garcia i Faria, 49-51, 08019, Barcelona, Spain

Abstract

A large number of problems in porous media frequently involve several coupled phenomena such as fluid flow, solute and heat transport, elastic and plastic mechanical deformations and geochemical reactions. Handling all the different physical and chemical processes and their interactions in a single model is not a simple task. We have developed a software interface, denoted as **iCP** (**i**nterface **C**OMSOL-**P**HREEQC), that aims at providing a flexible and efficient platform for the solution of large THCM (Thermo-Hydro-Chemical-Mechanical) problems. One of the main differences with other available software for coupled reactive solute transport simulations is that iCP allows using all the multiphysical capabilities of COMSOL Multiphysics ®, combined with the world class, well known geochemical simulator PHRREQC, developed at the USGS [1]. Scientific and technical details of the iCP tool has been recently published in the journal Computers & Geosciences [2], and the main structure and workflow of the interface can be seen in Figure 1.

During the past years, increasing interest has been raised in the understanding and modelling of the long-term behaviour of Engineered Barrier Systems (EBS) in the field of geological nuclear waste disposal. Sophisticated models are needed that can handle complex problems regarding the thermal, hydraulic, mechanical and geochemical evolution of such systems. Here, we present some examples of EBS models and customized stand-alone applications created with the Application Builder introduced in the latest Comsol Multiphysics V5.0 release.

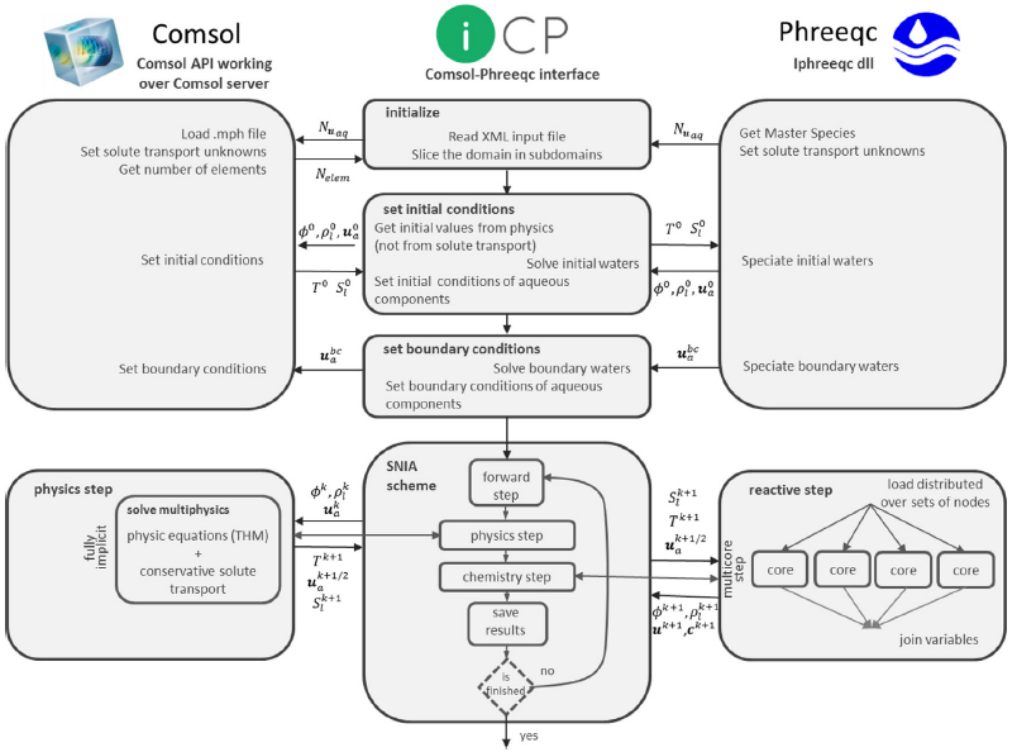

Figure 1. *Main structure and workflow of iCP. The most usual coupling (variable transfers) are shown in the chart, but iCP has been developed for general purpose simulations, without restrictions.*

References

[1] Parkhurst, D.L., Appelo, C.A.J., 1999. User's Guide to PHREEQC (version 2) *USGS Water-Resources Investigations Report* 99–4259. US Geol. Surv., Denver, Colorado, USA

[2] Nardi, A., Idiart, A., Trinchero, P., de Vries, L.M., Molinero, J. 2014. "Interface COMSOL-PHREEQC (iCP), an efficient numerical framework for the solution of coupled Multiphysics and geochemistry. *Computers & Geosciences* 69, pp10–21.

Analysis and Simulation of Thermal Energy Mechanism and Convection Processes in the Halls and Courtyards of the Alhambra in Granada

D. Blasco Avellaneda[*1], A. Martínez[2], D. Ruiz[1]

[1]Applied Physics Department, University of Granada, [2]ITCEA+
*Dpto. Física Aplicada, Facultad de Ciencias, Avda. Fuentenueva s/n 18001-Granada (Spain), blasco@ugr.es

Abstract

"It is really comfortable", often visitors to the Alhambra say. Why visit Alhambra experience is so pleasant? Not only for the artistic experience but also by the experience of thermal comfort inside the rooms. The courtyard as an architectural element is widespread along and across the Mediterranean geography, as a characteristic element of our culture. It is known to all and has been studied extensively the utility in light and ventilation control.

We analyzed this. We conducted a study of the elements of the Alhambra: walls, solar irradiance, thermal transmittance, thermal variability, and ventilation. We implemented a numerical model based on the finite elements method for analysis of computational fluid dynamics to conduct a study of convective flows, thermal gradients and energy performance in the courtyards and halls of the Alhambra of Granada.

We have used the software FreeFEM++. We will then develop COMSOL simulation models to support our results and expand the scope of analysis.

This study provides information to understand the phenomenon of large temperature difference between outside and inside, local thermal variability and the thermal comfort experience in the Alhambra.

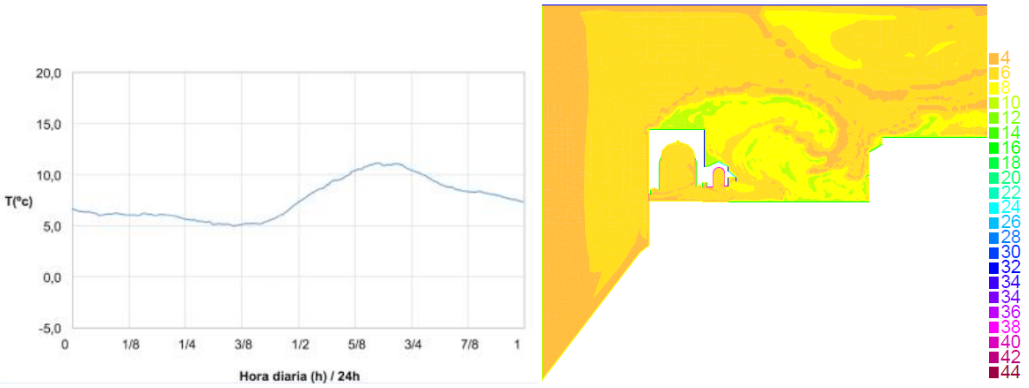

Figure 1. *Left: day temperature in one of the halls of the Alhambra. Right: Temperature distribution in a longitudinal central slice of Patio de los Arrayanes.*

Copper Slag-Matte Decantation Studies

C.Bontoiu[1*], I. Moreno-Ventas[1], M. Bacedoni[1], F.J.Blas[2]

[1] Departamento de Geología, Universidad de Huelva, 21071 Huelva,
[2] Departamento de Fisíca Aplicada, Universidad de Huelva, 21071 Huelva
*cristian.bontoiu@dfa.uhu.es

Abstract

Modelling the dynamics of copper slag-matte droplets has become an important issue of research with the advent of the new flash-smelter furnaces [1]. Better understanding of the thermal and chemical phenomena occurring at the interface between the two immiscible melts can improve the efficiency of the separation process. Preliminary studies of the decantation process of copper slag and matte are presented based on the Level Set method [2] implemented in COMSOL Multiphysics. The droplets are modelled as spheres of matte contained within slightly larger spheres of slag and released randomly in time with a statistical distribution of size, initial position and velocity. Depending on the surface tension coefficient, the analysis outlines findings on the amount and properties of matte drops caught within the slag layer.

Acknowledgments: The authors would like to express their gratitude to the Atlantic Copper Company based in Huelva (Spain) for funding the current research project and providing useful information.

References

[1] M.E. Schlesinger, M.J. King, K.C. Sole, and W.G. Davenport. Extractive Metallurgy of Copper. Elsevier Science, 2011.
[2] Elin Olsson, Gunilla Kreiss. A conservative level set method for two phase flow. Journal of Computational Physics, 210(1):225 – 246, 2005.

Abstracts Poster presentations

Ultrasonic Drying Design: Acoustic-Structure Interaction Modeling.

J. Bon*[1], V. Acosta[2], E. Riera[2], A. Pinto[2]

[1]Food Technology Department, Polytechnic University of Valencia
[2]Instituto de Tecnologías Físicas y de la Información (ITEFI), CSIC
*Food Technology Department, Polytechnic University of Valencia, Valencia 46022, Spain. jbon@tal.upv.es

Abstract

Introduction.- Power ultrasound is an attractive procedure for drying heat-sensitive foods (García-Pérez et al., 2006). The design of an ultrasonic drying (UD) requires the development of a high-power transducer and to study its interaction with the fluid media (Riera et al., 2004). The methodology and limitations found in this work are described in this presentation.

The application of a mathematical model, considering the interaction, would allow analyzing the influence of the variables on the sound field distribution. In this case, linear elastic models with attenuation for the acoustic-structure interaction modeled the transducer response and the acoustic pressure distribution inside the UD (Fig.1). To design the UD, the influence of the directivity of the drying open chamber and the staggered reflectors over the acoustic pressure distribution were investigated. Furthermore, to optimize the influence of the acoustic energy on the drying process, the average value of the acoustic energy (AE) distribution in the drying chamber, that would determine the adequate position of the food samples to be dried, was calculated.

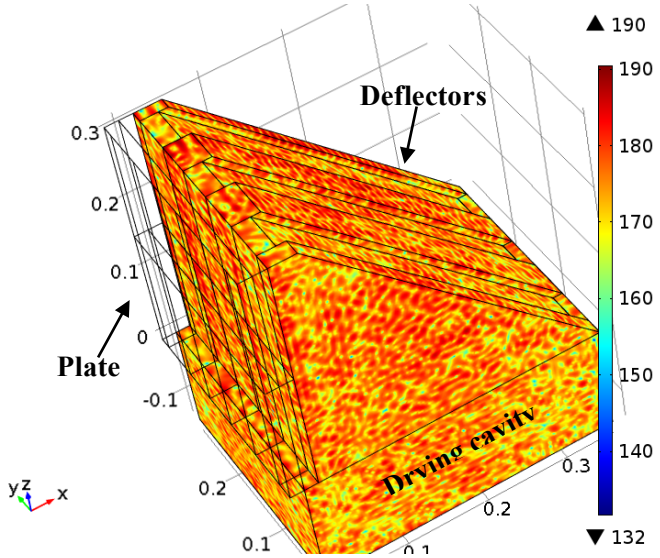

Figure 1. *Air pressure distribution (dB) in a quarter part of UD.*

Use of COMSOL Multiphysics.- COMSOL Multiphysics 5.0 was used to solve the mathematical model. For that, the Acoustic Pressure, Frequency Domain and the Solid Mechanic interfaces, coupled with the Multiphysics Node, were applied.

Numerical solution, applying the finite element method of acoustic-structure interactions involves to couple structural and fluid elements with different degrees of freedom, whose solutions imply several problems of hardware requirements and software configuration, which were solved considering several simplifications (Trujillo et al., 2011) and changing the available hardware.

To guarantee a good compromise between computational time and accuracy results, it was established that the element size should be shorter than a fifth of wavelength. Since the software needed more than 1000 Gb of memory to solve the model, the available hardware was modified, increasing to 250 Gb of RAM, and two SDD hard disks as virtual memory.

Results.- From the analysis of the transducer resonance modes the working frequency was obtained (20856 Hz).

Fig. 2 shows the evolution of the acoustic energy distribution and of the average pressure (P) (dB) in the drying cavity versus its height (H). There are several relative optimal points, and the absolute optimum value was 0.139 m.

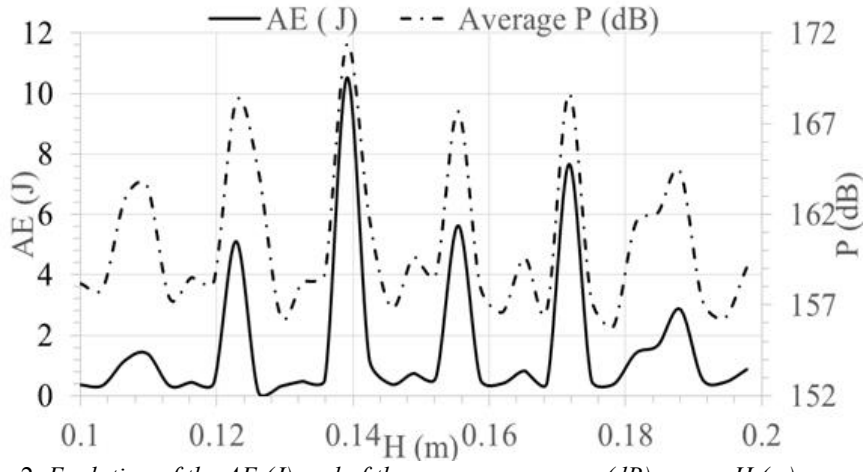

Figure 2. *Evolution of the AE (J) and of the average pressure (dB) versus H (m).*

Conclusion.- The UD designed produced high intensity and sound pressure levels in the drying cavity.

The application of the mathematical model would enable to optimize the UD designed sizing or the drying process operation, in order to maximize the influence of the sound field on the drying process. The acoustic energy distribution in the chamber would determine the adequate position of the food to be dried. For this purpose, the acoustic power absorbed by the samples will be analyzed in later studies.

References

1. García-Pérez, J.V., Cárcel, J.A., De la Fuente-Blanco, S., Riera-Franco de Sarabia, E. Ultrasonic drying of foodstuff in a fluidized bed: Parametric study. Ultrasonics 44, e539–e543. 2006.
2. Riera, E., Rodríguez, G., Vázquez, F., De la Fuente, S., Campos, C., Gallego, J.A. Development of a fluidized-bed dryer system assisted by power ultrasound, Contributed Paper, 9th Meeting of the European Society of Sonochemistry, April 25–30, Badajoz, Spain, Abstract Book OC-20, pp. 79–80.). 2004.
3. Trujillo, F.J., Knoerzer, K. Modeling the acoustic field and streaming induced by an ultrasonic horn reactor. In: Knoerzer, K., Juliano, P. Roupas, P., Versteeg, C. (Eds.) Innovative Food Processing Technologies: Advances in Multiphysics simulation. IFT Press and WILEY-BLACKWELL, Oxford, pp. 233-264. 2011.

Acoustic Studies of Bubble Chamber for Direct Dark Matter Searches

I. Felis[*1], M. Ardid[1]

[1]Polytechnical University of Valencia (UPV)
*C/Paraninf 1, 46730 Gandia, Valencia, ivfeen@upv.es

Abstract

Direct detection of dark matter is one of the most important topics in modern physics. It is estimated that 22% of universe matter is composed by dark matter in front of 4% of ordinary matter like stars, galaxies, planets and all kind of known astrophysical objects. PICO project [1], composed by COUPP and PICASSO researchers, aims to detect dark matter particles like WIMPs (Weakly Interacting Massive Particles) with the bubble chamber technique. The experiment is installed at a depth of 2 km in the SNOLAB underground laboratory at Sudbury, Ontario, Canada. The PICO collaboration is presently operating two dark matter search experiments: a bubble chamber filled with 37 kg of CF3I and a chamber loaded with 3 kg of C3F8. A much larger version of the experiment with 500 kg of active mass is in development.

The bubble chamber technique consist in a pressurized chamber filled with a fluid (in this case CF3I or C3F8) that operates in superheated regime. Detection of nuclear recoil is based on bubble formation. When nuclear recoil is produced with enough energy and this energy is deposed in the medium in a space smaller than the critical radius for a given thermodynamic conditions a macroscopic bubble is generated. This bubble produces an acoustic signal that is registered by piezoelectric transducer. Figure 1 shows the PICO 2L chamber and the 3D geometry.

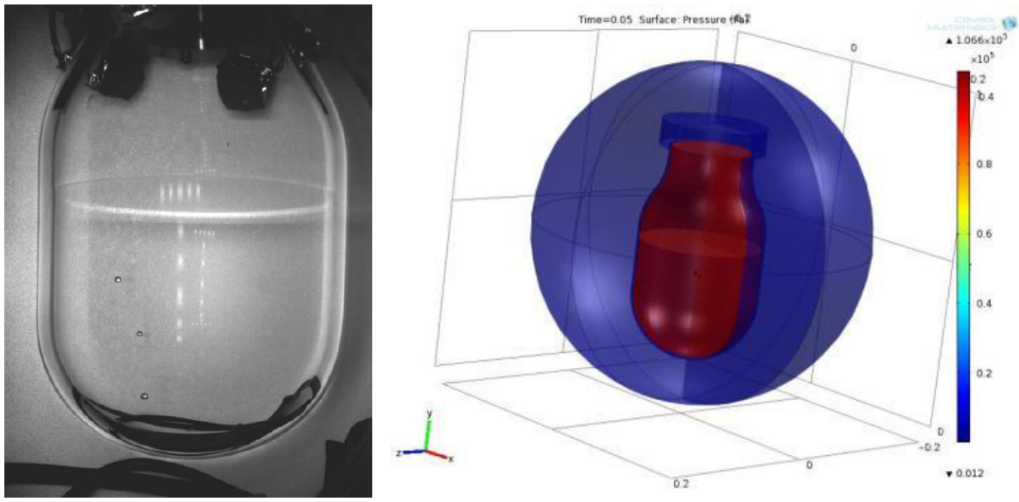

Figure 1. *Photography of PICO 2L chamber and the 3D geometry for simulation.*

To better understand the acoustic processes involved when a bubble grows we have made several simulations in COMSOL Multiphysics. Whit the Acoustic Module and Structural Mechanic Module, we have studied the generation, propagation and transmission of sound within the chamber and the increase of pressure due to the volume reduction when the bubble grows. Different like-bubble signals and more signal like sines and sweeps was the input in the bubble surface. The simulation was compared with the results of an experimental acoustic test bench developed in the Applied Physics Department of the UPV. Figure 2 shows some results of the acoustic propagations of different signals and the pressure increase in the chamber at different pressures inside the chamber.

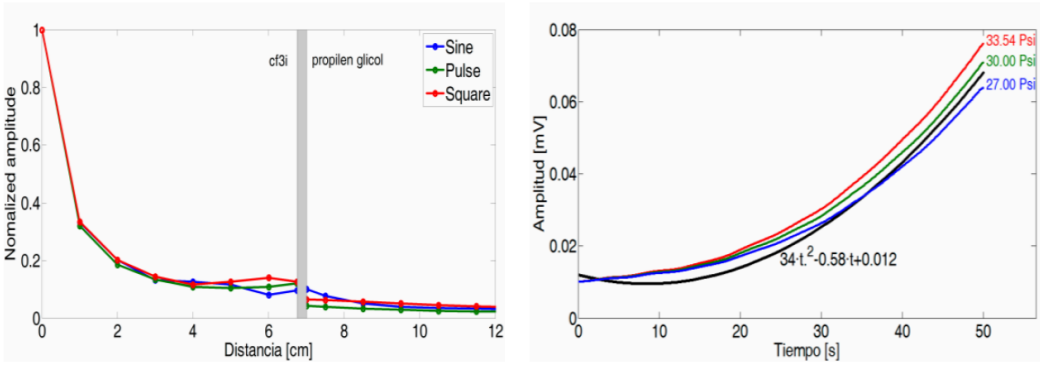

Figure 2. *Left: Propagation of acoustic signals within the chamber and through the bubble wall. Right: pressure increase within the chamber.*

The Acoustic-Piezoelectric Interaction multiphysics interfaces have been used to improve the design of the piezoelectric sensors attached to the chamber. Firstly, several types and geometries free ceramics was simulated (figure 3). Secondly, was studied these ceramics attached to the chamber. In addition, some matching layers were implemented to improve the sound transmission from the superheated fluid to the ceramics. All these simulation was compared with the measured of the electrical impedance.

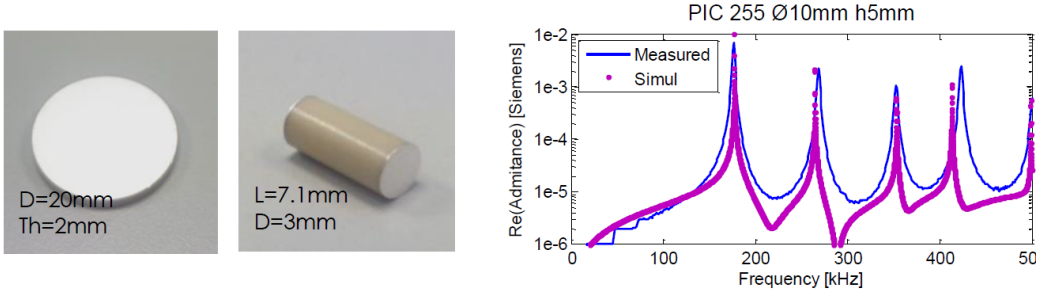

Figure 3. *Left: two of the piezoceramics simulated. Right: a simulation of one of them.*

References

1. http://www.picoexperiment.com/index.php
2. B. B. Mikic, W. M. Rohsenow, P. Griffith, *Int. J. Heat Mass Transfer* **13**, 657–665 (1970).
3. A. Arnau et al., *Piezoelectric Transducers and Applications*, 2th ed. Springer (2008).
4. J. Riznic, G. Kojasoy, N. Zuber, *Int. J. Fluid Mech. Res*. **26**, 110–145 (1999).
5. M.Bou, I.Felis, M.Ardid, *LRT2013. AIP Conference Proceedings*, **1529**, 142–147 (2013).

Copper Slag-Matte Decantation Studies

C.Bontoiu[1*], I. Moreno-Ventas[1], M. Bacedoni[1], F.J.Blas[2]

[1] Departamento de Geología, Universidad de Huelva, 21071 Huelva,
[2] Departamento de Fisíca Aplicada, Universidad de Huelva, 21071 Huelva
*cristian.bontoiu@dfa.uhu.es

Abstract

Modelling the dynamics of copper slag-matte droplets has become an important issue of research with the advent of the new flash-smelter furnaces [1]. Better understanding of the thermal and chemical phenomena occurring at the interface between the two immiscible melts can improve the efficiency of the separation process. Preliminary studies of the decantation process of copper slag and matte are presented based on the Level Set method [2] implemented in COMSOL Multiphysics. The droplets are modelled as spheres of matte contained within slightly larger spheres of slag and released randomly in time with a statistical distribution of size, initial position and velocity. Depending on the surface tension coefficient, the analysis outlines findings on the amount and properties of matte drops caught within the slag layer.

Acknowledgments: The authors would like to express their gratitude to the Atlantic Copper Company based in Huelva (Spain) for funding the current research project and providing useful information.

References

[1] M.E. Schlesinger, M.J. King, K.C. Sole, and W.G. Davenport. Extractive Metallurgy of Copper. Elsevier Science, 2011.
[2] Elin Olsson, Gunilla Kreiss. A conservative level set method for two phase flow. Journal of Computational Physics, 210(1):225 – 246, 2005.

Microfluidic Cell Trapping Device for Single-Cell Studies

C. Freitas[1,2*], C. Mendes[2], F. Pereira[1,2], E. Fortunato[1],
R. Martins[1], H. Águas[1], A. Oliva[2,3]

[1]CENIMAT/I3N, Departamento de Ciência dos Materiais, Faculdade de Ciências e Tecnologia, Universidade Nova de Lisboa and CEMOP-UNINOVA, 2829-516 Caparica, Portugal.
[2]Instituto de Tecnologia Química e Biológica - Universidade Nova de Lisboa. 2781-901 Oeiras, Portugal.
[3]Instituto de Biologia Experimental e Tecnológica, 2781-901 Oeiras, Portugal.
*catarinacdefreitas@gmail.com

Abstract

Introduction.- We developed a microfluidic platform to study living cells at the individual level. Our device consists in a polydimethylsiloxane (PDMS) chip with micro-channels containing arrays of V and U-shaped hydrodynamical traps where cells are immobilized and its response to bio- and chemical stimuli can be monitored in real time with inverted microscopy imaging. We engineered devices with two configurational sizes to be used with two types of cells: blood cells (5-10µm) and plant cells (50-100µm). This platform will be used to study the advantages of fluorescent nanoparticles (Quantum Dots, QDs) as labels for imaging. We will evaluate the cytotoxic effect of the nanoparticles on the cells and study of migration of QDs inside them, at the same time that environmental parameters such as nutrients, pH, temperature, etc. are modulated.

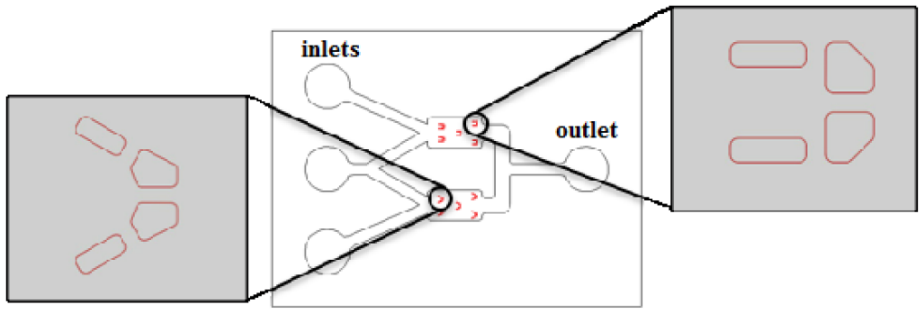

Figure 1. *Example of a chip structure with two different conformations of traps. Cells are introduced in the central inlet whereas buffer solution is added to the lateral inlets. Samples are controlled by pressure driven flow.*

Computational simulations are a powerful tool to test microfluidic chips design efficiency before proceeding to fabrication, saving time and resources, as well as to guide experimental operation. We used COMSOL Multiphysics to study flow velocity

fields and pressure fields and we used the results to optimize channel dimensions and geometry of traps.

Since channels have rectangular cross section, a 2D simulation with a channel shallow approximation was used. Structures layouts were imported from AutoCad to COMSOL and the default relative repair tolerance was set to 1,0E-6. The Creeping Flow Module was used since the flow is laminar and the liquid was assumed as incompressible. In all domains the used liquid was water and null initial conditions were set. In addition, the no-slip condition was set for all walls. The mesh was automatically built by COMSOL ("Physics-controlled mesh") with an element size as fine as possible that can varies because of the complexity of designs and the available memory in the computer. The problems were solved using PARDISO.

Results.- Our microfluidic platform successfully captured cells and allowed cell monitoring during biological experiments.

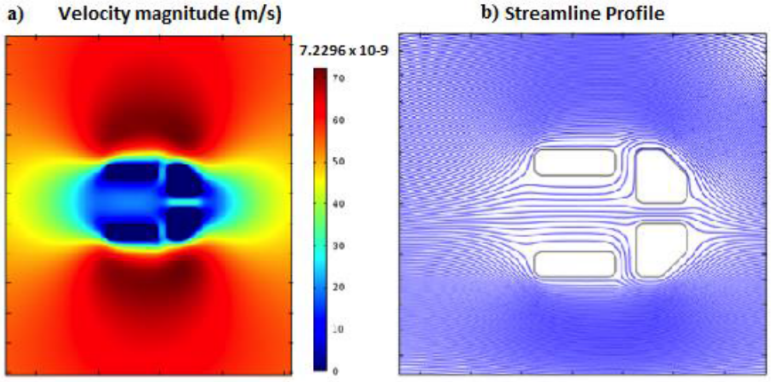

Figure 2. *Simulation results from COMSOL. a) Rainbow color represents the flow velocity magnitude distribution. b) Streamlines indicate the flow direction around and through a trap.*

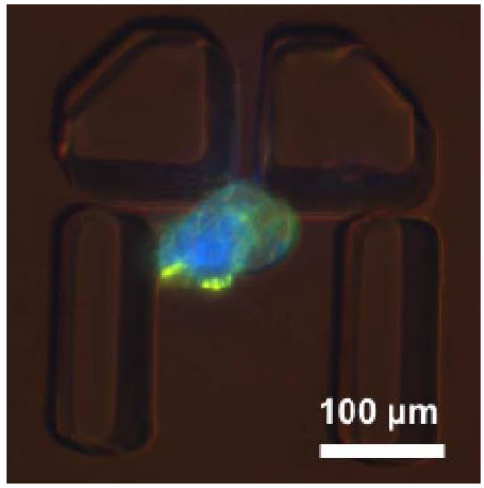

Figure 3. *Fluorescent microscopy results of a plant cell trapped after a 2 hours assay with Quantum Dots*.

Conclusion.- Single-cell analysis has advantages over traditional bulk measurements, since it allows studying cell heterogeneity in a population of cells instead of averaging cell characteristics. We have used COMSOL to optimize the design of our microfluidic platform for cell trapping and the produced device proved efficient during our studies. In the future, this platform is going to be used in additional experiments developed in our lab with virus and parasites.

References

1. Zare, Richard N., and Samuel Kim, Microfluidic platforms for single-cell analysis, *Annual review of biomedical engineering,* **12**, 187-201 (2010).
2. Lecault, Véronique, et al., Microfluidic single cell analysis: from promise to practice, *Current opinion in chemical biology,* **16.3**, 381-390 (2012).
3. Wheeler, Aaron R., et al., Microfluidic device for single-cell analysis, *Analytical chemistry*, **75.14**, 3581-3586 (2003).

Three-Dimensional Modeling of Scanning Microwave Microscopy Applied to a Single Bacterial Cell

R. Fabregas[1], M. C. Biagi[*1], L. Fumagalli[3], G. Gomila[1,2]

[1]Institut de Bioenginyeria de Catalunya (IBEC).
[2]Departament d'Electrònica, Universtat de Barcelona.
[3]School of Physics and Astronomy, The University of Manchester.
*Institut de Bioenginyeria de Catalunya (IBEC), 08028 Barcelona, Spain, mcbiagi@ibecbarcelona.eu

Abstract

Scanning Microwave Microscopy (SMM) is a powerful tool to investigate the local electrical polarization of materials with micro and nanoscale lateral precision [1, 2]. This technique consists in mapping the local impedance of materials with the use of evanescent microwaves emitted and collected by a sharp tip, which is scanned above the sample surface. In such a way, the great lateral resolution of the near-field measurements (far below the optical limit) is combined with the high penetration depth of the microwaves [2, 3].

Yet, in order to obtain quantitative intrinsic information about the dielectric properties of the sample (i.e. permittivity and conductivity), the SMM impedance measurements must be combined with a theoretical model accounting for the geometrical effects of the probe-sample system.

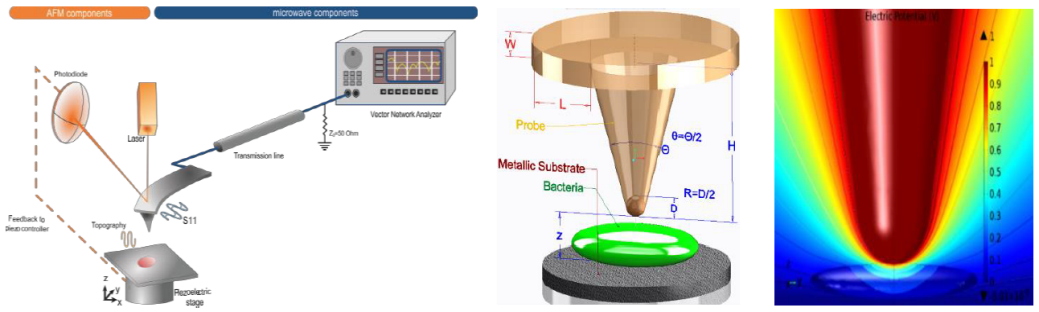

Figure 1. *(a) Schematic representation of the Scanning Microwave Microscopy setup. (b) Schematic representation of the 3D model used in the finite element numerical calculations. (c) Electric potential distribution obtained from the COMSOL Multiphysics simulation.*

Here, we present the three-dimensional model of the SMM probe used to calculate the impedance of the tip-single bacterium cell. The SMM tip is modelled as a cone ending with a semi-sphere (tip apex), whereas the bacterium, lying on a metallic substrate, is modelled as an oblate ellipsoid (Figure 1(b)). The AC/DC electrostatic module of COMSOL Multiphysics 5 was used to solve the static electric field between

tip and bacterium at various distances, in a cylindrical domain with an infinite elements layer on the boundary (see Figure1(c)). From the field distribution, the charge density on the tip surface, and therefore the capacitance, can be derived. The conductance was not included in the model, as it appeared from the experiment to be fully negligible.

We show here that interpreting the experimental measurements with the theoretical calculations by this model can provide quantitative values for the bacterium permittivity in the GHz domain for the first time.

The model presented here can be adapted to a number of different applications. First, it can be used to mimic also the electrostatic force microscopy setup, where the capacitance gradient is measured. Then, in the so-called nanotomography problems, the model can enable the reconstruction of sub-surface electrical images, which can be used to interpret the experimental data in order to retrieve the internal dielectric properties from surface measurements.

References

1. Esteban-Ferrer, D., Edwards, M. A., Fumagalli, L., Juan, A. & Gomila, G. Electric, Polarization Properties of Single Bacteria Measured with Electrostatic Force Microscopy, ACS Nano, 8, 9843-9849 (2014).
2. Ghamsari, B. G. & Anlage, S. M., Nanoscale Electrodynamic Response of Nb Superconductors, EEE Trans. Appl. Supercond*,* 23**,** 7100104-7100104 (2013).
3. Lee, J., Long, C. J., Yang, H., Xiang, X.-D. & Takeuchi, I., Atomic resolution imaging at 2.5 GHz using near-field microwave microscopy, Appl. Phys. Lett., 97, 183111 (2010).
4. Plassard, C. *et al*., Detection of defects buried in metallic samples by scanning microwave microscopy, Phys. Rev. B, 83, 121409 (2011).

Numerical Simulation of Piezoceramic Elements

J. Barreiro[1], A. Saenz de Inestrillas [1], F. Camarena[1]

[1]Universitat Politècnica de València. Institut d'Investigació per a la Gestió Integrada de les Zones Costaneres.
* EPSG. C/Paranim 1, 46730 Grau de Gandia. fcamarena@fis.upv.es

Abstract

The Piezoelectric Ceramics are characterized by their excellent capacity of transduction, converting a deformation of their structure in a voltage (Direct piezoelectric effect) or an electric stimulation in a structural deformation (Inverse piezoelectric effect). Their working bandwidth and the impedance resonance frequencies are conditioned by mechanical and electric losses coefficients, matrices that define the properties mechano-acoustics and electro-mechanics, the geometry, and the ceramics' poling direction. Getting a good characterization of the impedance and admittance is important in order to design and develop optimized transducers.

COMSOL Multiphysics with it Piezoacoustic module is used aiming to validate a simulation model that allow to know the impedance and admittance of three different sizes of PIC 255 ceramics, Figure 1, taking into the account the damping and losses condition into the Domain condition of Piezoelectric material interface, as well as input parameter mentioned above, in order to be used at the time to design and simulate a bandwidth transducer optimized both in emission and reception as well to get an approximation in sensibility.

Simulation Match with the experimental results for a PIC 255 ceramic, Figure 2. All the above could be possible if the parameters of the ceramic are delivery by the manufacturer. Another important parameter in order to get a more accurate approximation in the amplitude of the resonance, are the mechanical and electrical damping and losses coefficients, all of them despite that the manufacturer bring this values, it is necessary to manual tuning until get a better approximation.

Figure 1. *From left to right - ceramic 1, ceramic 2 and ceramic 3.*

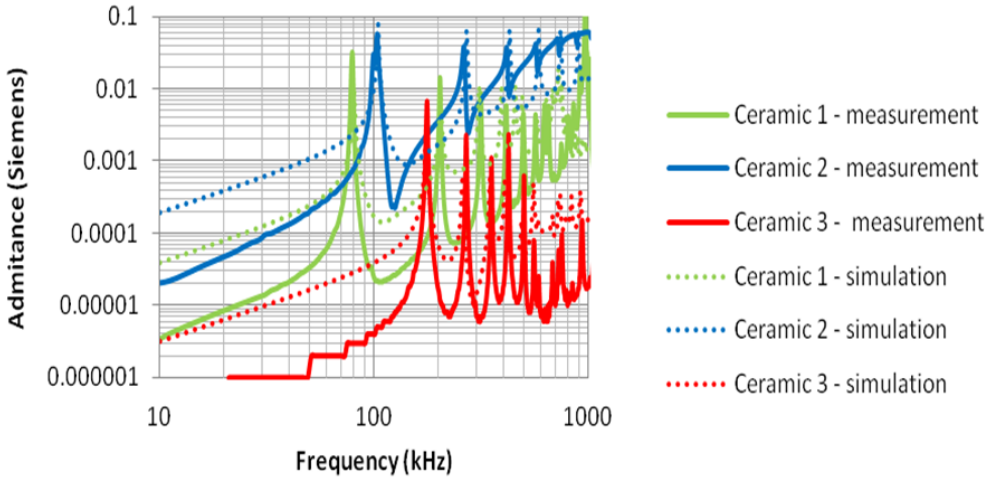

Figure 2. *Ceramics' Admittance. Measurement and Simulation.*

References

1. Kinsler, Lawrence E et al. "Fundamentals of acoustics." *Fundamentals of Acoustics, 4th Edition, by Lawrence E. Kinsler, Austin R. Frey, Alan B. Coppens, James V. Sanders, pp. 560. ISBN 0-471-84789-5. Wiley-VCH, December 1999.* 1 (1999).
2. Lerch, Reinhard. "Simulation of piezoelectric devices by two-and three-dimensional finite elements." *Ultrasonics, Ferroelectrics, and Frequency Control, IEEE Transactions on* 37.3 (1990): 233-247.

Papers

Geometry Induced Biofilm Formation

A. Carpio[1,*], D. R. Espeso[2]

[1]Departamento de Matemática Aplicada, Universidad Complutense de Madrid, 28040, Spain
[2]Centro Nacional de Biotecnología, CSIC, Spain, 28049
*Corresponding author: carpio@mat.ucm.es

Abstract: Bacteria in aqueous environments usually gather to form aggregates called biofilms. In biofilms, cells display many behavioral differences from planktonic cells, such as a 1,000-fold increase in tolerance to antibiotics. Hospital-acquired infections are often caused by biofilm spread through medical systems. Design improvements hindering biofilm formation rely on identifying factors that favor their appearance. Geometry variations in medical flow circuits may trigger biofilm nucleation through vortical motion driving bacteria to walls.
Detailed flow studies in mili and microfluidic devices support that observation. Once biofilm seeds are created, they proliferate forming filaments whose structure is again controlled by the geometry.

Keywords: Biofilms, flows, hospital acquired infections.

1. Introduction

Biofilms are the dominant habitat of bacteria in nature: clusters formed by bacteria attached to each other and to a moist surface, enveloped by a polymeric matrix produced by bacteria themselves [1,2], see Figure 1. In their biofilm form bacteria are extremely resistant to external aggressions by chemicals, disinfectants, antibiotics and flows. For that reason, biofilms are a main cause of hospital acquired infections [1].

Most antibiotics have been designed to target floating bacteria. Survivors are then eliminated by our immune system. In biofilms, the polymeric matrix prevents the immune system from eliminating survivors. A chronic infection develops. Antibiotics do not succeed in killing all bacteria for a variety of reasons [2]. They may fail to penetrate deep inside the biofilm through the polymeric matrix. Bacteria within the biofilm may mutate, avoiding the antibiotic action.

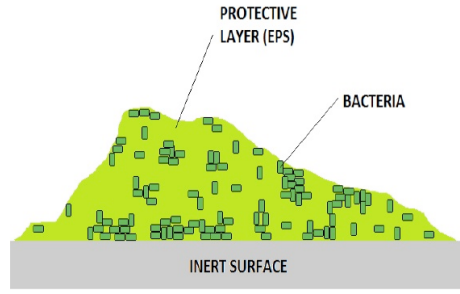

Figure 1. *Schematic representation of a biofilm. A polymeric matrix formed by exopolysaccharides (EPS) envelops bacteria attached to a moist surface.*

Hospital acquired infections are the result of a vicious cycle. Microbes live in the hospital environment, on the patient himself and on the medical equipment. The medical staff and

invasive devices act as vehicles that introduce microbes inside the body. Most hospital acquired infections are triggered by implants: artificial joints, vascular grafts, heart valves, catheters…

As the life expectancy increases, the possibility of requiring medical implants grows. 7% more implants are performed every year. This results in an increasing number of infections, specially in immunocompromised patients (about 2 million a year in the USA), huge economic costs for the health care system, and a percentage of avoidable deaths [3]. Understanding how the design of medical equipment influences biofilm nucleation and growth may help to reduce this trend.

The role of the geometry in biofilm nucleation in flow circuits has been pointed out in Ref. [4,5]. Experimental studies in laminar corner microflows show that biofilms nucleate at corners, forming filaments that cross the mainstream [4,6]. COMSOL studies of the structure of the flow relate this fact to the presence of secondary vortices driving floating bacteria to the walls [4]. Experimental and numerical studies also show the formation of helical biofilm threads past narrowings [5], driven by vortices. Studying the structure of the flow, we may infer which geometrical features trigger biofilm nucleation. The shape of the resulting biofilm filament is decided by the interaction of the flow with the growing elastic thread [6,5]. Coupling simulations of corner flows with cellular automata descriptions of aggregation processes, 3D structures crossing the mainstream are generated [7]. More realistic descriptions of the process consider the biofilm a thin filament interacting with the flow [6,5]. COMSOL studies of flows in specific geometries combined with MATLAB simulations of filaments actuated by the flow [6,5,8] provide a flexible tool to predict biofilm nucleation and spread in flow circuits. Instead, predictions of biofilm spread over surfaces relies on plate deformation analysis [9]. We focus here on analyzing geometric features that may trigger biofilm formation in flows.

2. Governing equations

Medical flow circuits usually consist of networks of tubes, with a diameter of a few milimiters, that circulate fluids carrying mixtures of substances from a reservoir into a patient.

Figure 2 illustrates a simple lay out. The flow is set in motion through a drip mechanism, or a roller pump, that induces slow pulsatile flows not harming cells.

Figure 2. *Lay-out for a standard circuit, formed by a reservoir, a pump and a network of interconnected tubes.*

Typical alterations of the tube cylindrical geometry occur at junctions, to split or merge branches (T-junctions), to connect conduits of different diameters, or to attach tubes to

different elements of the circuits. Our simulations target regions where the cylindrical shape is altered. The fluid flow in the selected geometry is governed by the incompressible Navier-Stokes equations:

$$\rho\frac{\partial \mathbf{u}}{\partial t} - \nabla \cdot \eta(\nabla \mathbf{u} + (\nabla \mathbf{u})^T) + \rho \mathbf{u} \cdot \nabla \mathbf{u} + \nabla p = 0$$

$$\nabla \cdot \mathbf{u} = 0$$

where **u** denotes the velocity (m/s), p the pressure (Pa), ρ the density (kg/m^3) and η the viscosity (N·s/m^2). Neglecting viscosity and density variations due to the presence of bacteria and chemicals in the fluid we will set the viscosity equal to 10^{-3} N·s/m^2 and a density of 10^3 kg/m^3. On the walls of the tube we impose no slip boundary conditions: **u** = 0.

3. COMSOL Model and Results

The basic geometries under study are conduits of varying diameters, as in Figures 3 and 4, where tubes of 2 mm and 4 mm are connected.

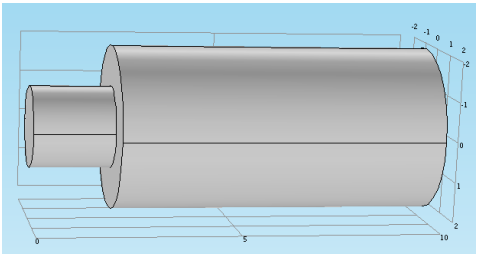

Figure 3. *Straight connection between tubes of different diameters.*

Typical maximum flow velocities are 1 mm/s. Reynolds numbers are of order one. The flow is described by a laminar regime, and set in motion by a pressure drop, imposed through a pressure jump between inlet and outlet. The velocity component *w* in the direction parallel to the tube walls develops a typical Poiseuille profile after the narrowing, see Figure 5.

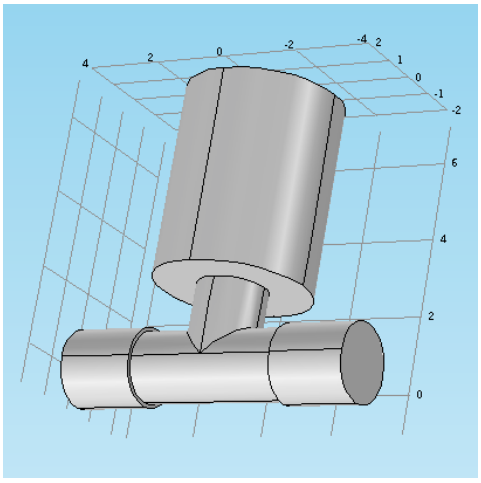

Figure 4. *T-junction used to merge or split conduits.*

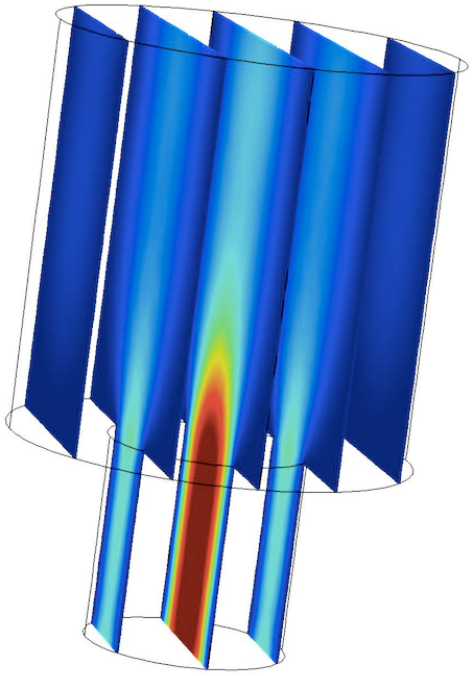

Figure 5. *Slices depicting the spatial variation of the w component of the velocity (parallet to the wall) past the narrowing*

represented in Figure 3. The velocity modulus shows a similar profile.

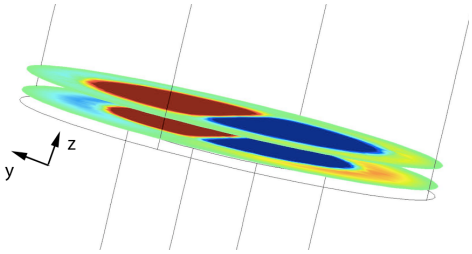

Figure 6. *Slices indicating the sign of the velocity in the direction y, orthogonal to the walls, which suggests recirculation in the vortex region. Colors evolve from blue (negative) to red (positive).*

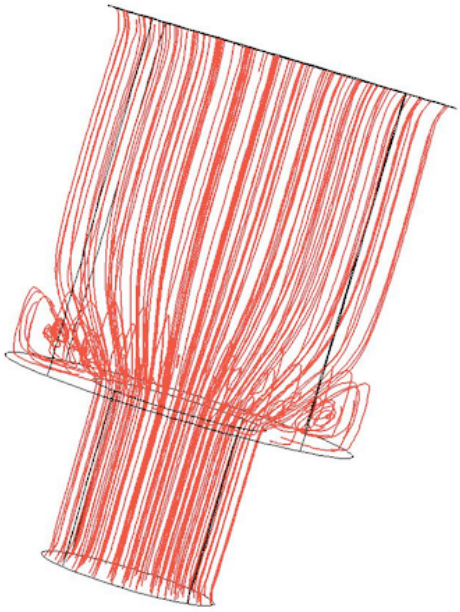

Figure 7. *Streamlines illustrating vortex formation past the narrowing depicted in Figure 3. Floating bacteria are driven to the walls forming biofilms.*

The magnitude of the components of the velocity in the direction orthogonal to the walls is 10 times smaller. However, a careful study shows changes of sign past the narrowing, which indicates recirculation, see Figure 6. Depicting the streamlines, we observe streamline expansion and the appearance of vortices, see Figure 7. Floatings cells may be trapped by these eddies and driven to the walls of the tubes. Those areas become preferential sites for biofilm nucleation.

Figures 5-7 correspond to a constant drop pressure, that creates a steady flow. A pulsatile flow can be simulated by imposing a periodic drop. A similar structure is observed, but the magnitude of the velocity components increases and decreases periodically, see Figure 8. The vortices undergo slight periodic expansions and contractions too.

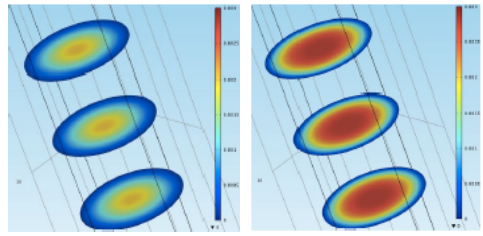

Figure 8. *Fluctuations of the velocity modulus along the tube at different instants of a period of a pulsatile flow.*

Once the microorganisms reach the walls, successful attachment depends on the material forming the tubes and the bacterial strain. When a biofilm seed is created, it is shaped by the current, producing threads elongating downstream. As these threads become longer, they interact with the flow, adopting different equilibrium shapes [6,5]. The spread of the biofilm threads can be described by means of rod models that compute the evolution of a filament subject to the

forces exerted by the flow [6,5].

5. Conclusions

Detailed studies of the flow structure in specific geometries may predict preferential sites for biofilm nucleation in medical flow systems, usually regions where vortices perturbing the primary laminar flow and driving particles to walls are formed. Combining flow simulations with elastic rod descriptions we may predict the spread and structure of nucleated biofilm filaments.

Tube geometry variations, such as narrowings and corners, should be avoided in medical circuits to reduce the risk of biofilm nucleation. If unavoidable, antimicrobial protocols should target them.

6. References

1. K. Vickery, H. Hu, A. S. Jacombs, D. A. Bradshaw, A. K. Deva, A review of bacterial biofilms and their role in device-associated infection, Healthcare Infection, 18, 61-66 (2013)
2. N. Hoiby, T. Bjarnsholt, M. Givskov, S. Molin, O. Ciofu, Antibiotic resistance of bacterial biofilms, Int. J. Antimicrob. Agents, 35, 322-332 (2010)
3. P. W. Stone, Economic burden of healthcareassociated infections: An American perspective, Expert. Rev. Pharmacoeconomics Outcomes Res., 9, 417-422 (2009)
4. R. Rusconi, S. Lecuyer, L. Guglielmini, H. A. Stone, Laminar flow around corners triggers the formation of biofilm streamers, J. R. Soc. Interface, 7, 1293-1299 (2010)
5. D.R. Espeso, A. Carpio, E. Martinez-Garcia, V. de Lorenzo, Stenosis triggers spread of helical Pseudomonas biofilms in cylindrical flow systems, preprint (2015)
6. N. Autrusson, L. Guglielmini, S. Lecuyer, R. Rusconi, H.A. Stone, The shape of an elastic filament in a two-dimensional corner flow, Phys. Fluids, 23, 063602 (2011)
7. A. Carpio, B. Einarsson, D. R. Espeso, Dynamics of bacterial aggregates in microflows, Progress in Industrial Mathematics at ECMI 2014, Springer, to appear
8. M. Bergou, M. Wardetzky, S. Robinson, B. Audoly, E. Grinspun, Discrete elastic rods, ACM Transactions on Graphics, 27, 63 (2008)
9. D.R. Espeso, A. Carpio, B. Einarsson, Differential growth of wrinkled biofilms, Phys. Rev. E, 91, 022710 (2015)

7. Acknowledgements

Research supported by grant No. FIS2011-28838-C02 of the spanish MICINN.

Simulation and optimization of High-Pressure/Temperature food treatments by using Comsol Multiphysics

J.A. Infante[1], B. Ivorra[1,*], J. López Redondo[2],
P. Martínez Ortigosa[2], Á.M. Ramos[1], J.M. Rey Cabezas[1]

[1]Universidad Complutense de Madrid.
[2]Universidad de Almería.
*Corresponding author: U.C.M., Fac. C.C. Matemáticas, Dpto. Matemática Aplicada, Plaza ciencias 3, 28400, Madrid – email: ivorra@mat.ucm.es

Abstract: High Pressure (HP) Processing has turned out to be very effective in order to prolong the shelf life of some foods. This paper deals with the modeling, simulation and optimization of the effect of the combination of high pressure with thermal treatments on food. In particular, we propose a mathematical formulation of an optimization problem which aims to control the food sample temperature according to the pressure evolution. Then, we propose a particular optimization algorithm to solve it. We note that this work is in progress and the optimization problem will be solved in the next future. The models developed here provide useful tools to design suitable industrial equipments and processes.

Keywords: Food engineering; High-Pressure/Temperature food treatment; Mathematical Modeling; Optimization.

1. Introduction

At present, the demand of safe and minimally processed food, prepared for immediate consumption (ready–to–use and ready–to–eat) has increased significantly, in order to give service to the needs of restaurants, collective dining rooms (colleges, companies, hospitals, residences, etc.) as well as to domestic consumption.

One of the technologies that can be used for the preparation of these products is High Pressure (HP) Processing, which has turned out to be very effective in order to prolong the shelf life of some foods (cooked ham, juices, guacamole, oysters, etc.) being already a reality at industrial level. These treatments have the great advantage of not being based on the incorporation of additives, which consumers prefer to elude. Furthermore, they allow to avoid treatments with high temperatures (as Pasteurization), which have adverse effects on some nutritional properties of the food, its flavor, etc. (see, e.g., [4] and [5]).

This paper deals with the modeling, simulation and optimization of the effect of the combination of high pressure with thermal treatments on food. These models may be very important in order to be able to design suitable industrial devices and processes.

Here, we first propose a mathematical model allowing predicting the temperature evolution of a food sample when the pressure is

known. Then, we formulate a particular optimization problem which aims to control the food sample temperature according to the pressure evolution. This problem will be solved in future work with a particular global optimization algorithm proposed at the end of this document.

2. Heat and Mass Transfer Modelling

When HP is applied in Food Technology, it is necessary to consider thermal effects produced by variations of temperature due to the work of compression/expansion in both the food and the pressurizing fluid.

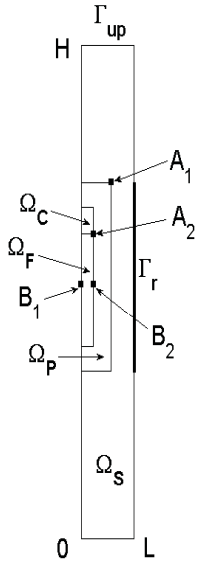

Figure 1. *Computational domain.*

After compression, heat exchange appears between the pressure chamber, the pressure medium and the food sample giving a time–dependent distribution of temperatures. In the fluid media (the pressurizing fluid and also the food when it is in liquid state) changes in temperatures imply changes in fluid density leading to free convection during the high pressure process. Therefore, conduction and convection have been considered in the models, taking into account heat and mass transfer (see [1,2,3,8]).

Often, HP experiments are carried out in a cylindrical pressure vessel (typically a hollow steel cylinder) previously filled with the food and the pressure medium. The sample is located in the inner chamber at a temperature that can be the same or different to the one in the pressure medium and/or the solid domain surrounding it, which may cool or warm the food following user's criteria.

The axial symmetry of the model allows us to consider cylindrical coordinates and the domain given by half a cross section (intersection of the cylinder with a plane containing the axis). Let us consider four bi-dimensional sub–domains (see Figure 1):

- Ω_F: domain where the sample of food is located.
- Ω_C: cap of the sample holder (typically a rubber cap).
- Ω_P: domain occupied by the pressurizing medium.
- Ω_S: domain of the steel surrounding the above domains.

Our domain in the (r,z)–coordinates is the rectangle $\Omega=[0,L] \times [0,H]$ defined by $\Omega = \Omega_F \cup \Omega_C \cup \Omega_P \cup \Omega_S$, where $\{0\}\times (0,H)$ generates the axis of symmetry. In the boundary of Ω, which is denoted by Γ, we distinguish:

- $\Gamma_r \subset \{L\}\times(0,H)$, where the temperature will be known.
- $\Gamma_{up} = [0,L] \times \{H\}$, where heat transfer with the room where

the equipment is located could take place.

- $\Gamma\backslash\{\Gamma_r \cup \Gamma_{up}\}$, with zero heat flux, either by axial symmetry or by isolation of the equipment.

We denote by Ω^*, Ω_F^*, Ω_C^*, Ω_P^*, Ω_S^*, Γ, Γ_r^*, Γ_{up}^* the domains generated when rotating Ω, Ω_F, Ω_c, Ω_P, Ω_s, $\Gamma\backslash\{0\}$x$(0,H)$, Γ_r and Γ_{up} along the axis of symmetry (in the 3D space), respectively.

2.1 Liquid food modeling

For the mathematical model we will consider a liquid type food. We propose a model considering convection both in the pressurizing medium and the region Ω_F. We distinguish two separated velocity fields $\mathbf{u_F}$ and $\mathbf{u_P}$ for the food and the pressurizing fluid, respectively.

The governing equations are

$$\begin{cases} \rho C_p \dfrac{\partial T}{\partial t} - \nabla\cdot(k\nabla T) + \rho C_p \mathbf{u}\cdot\nabla T \\ \quad = \alpha \dfrac{dP}{dt} T \text{ in } \Omega^*\times(0,t_f), \\ \rho \dfrac{\partial \mathbf{u_F}}{\partial t} - \nabla\cdot\eta(\nabla\mathbf{u_F} + \nabla\mathbf{u_F^t}) \\ \quad +\rho(\mathbf{u_F}\cdot\nabla)\mathbf{u_F} \\ \quad = -\nabla p - \nabla\cdot\left(\dfrac{2\eta}{3}(\nabla\cdot\mathbf{u})I\right) \\ \quad -\rho\mathbf{g} \text{ in } \Omega_F^*\times(0,t_f), \\ \rho \dfrac{\partial \mathbf{u_P}}{\partial t} - \nabla\cdot\eta(\nabla\mathbf{u_P} + \nabla\mathbf{u_P^t}) \\ \quad +\rho(\mathbf{u_P}\cdot\nabla)\mathbf{u_P} \\ \quad = -\nabla p - \nabla\cdot\left(\dfrac{2\eta}{3}(\nabla\cdot\mathbf{u})I\right) \\ \quad -\rho\mathbf{g} \text{ in } \Omega_P^*\times(0,t_f), \\ \dfrac{\partial\rho}{\partial t} + \nabla\cdot(\rho\mathbf{u_F}) = 0 \text{ in } \Omega_F^*\times(0,t_f), \\ \dfrac{\partial\rho}{\partial t} + \nabla\cdot(\rho\mathbf{u_P}) = 0 \text{ in } \Omega_P^*\times(0,t_f), \end{cases} \quad (1)$$

where P is the pressure (Pa) applied by the equipment, p is the pressure (Pa) generated by the mass transfer inside the fluid, T is the temperature (K), ρ is the density (kg·m^{-3}), C_p is the heat capacity (J·kg^{-1}·K^{-1}), k is the thermal conductivity (W·m^{-1}·K^{-1}), t_f (s) is the final time, η is the dynamic viscosity (Pa·s), g is the gravity vector (m·s^{-2}) and α is given by

$$\alpha = \begin{cases} \text{thermal expansion coefficient } (\mathrm{K}^{-1}) \\ \text{of the food in } \Omega_F^*, \\ \text{thermal expansion coefficient } (\mathrm{K}^{-1}) \\ \text{of the pressure fluid in } \Omega_P^*, \\ 0, \text{ elsewhere.} \end{cases}$$

We point out that the pressure medium and the food are separated by the sample holder and do not mix. Right hand term of first equation in (1) results from the following law:

$$\frac{\Delta T}{\Delta P} = \frac{\alpha T V}{M C_p} = \frac{\alpha T}{\rho C_p},$$

where ΔT is the change of temperature due to a change of pressure ΔP, V is the volume and M is the mass.

We also consider the following point, boundary and initial conditions:

$$\begin{cases} k\dfrac{\partial T}{\partial \mathbf{n}} = 0 \text{ on } \Gamma^*\backslash(\Gamma_r^*\cup\Gamma_{up}^*)\times(0,t_f), \\ k\dfrac{\partial T}{\partial \mathbf{n}} = h(T_{amb} - T) \text{ on } \Gamma_{up}^*\times(0,t_f), \\ T = T_{ref} \text{ on } \Gamma_r^*\times(0,t_f), \\ \mathbf{u_F} = 0 \text{ on } \Gamma_F^*\times(0,t_f), \\ \mathbf{u_P} = 0 \text{ on } \Gamma_P^*\times(0,t_f), \\ T = T_0 \text{ in } \Omega^*, \\ p = 10^5 \text{ in } A_1\times(0,t_f), \\ p = 10^5 \text{ in } A_2\times(0,t_f), \end{cases} \quad (2)$$

where Γ_F^* denotes the boundary of Ω_F^*, Γ_P^* is the boundary of Ω_P^*, A_1, A_2 are corner points of Γ_P^* and Γ_F^*, respectively

(see Figure 1), **n** is the outward normal vector on the boundary of the domain, T_0 us the initial temperature, T_{ref} is the temperature that is kept constant in Γ_r^* (cooling or warming the food sample), T_{amb} is the (constant) temperature at the external environment and h ($\text{W}\cdot\text{m}^{-2}\cdot\text{K}^{-1}$) is the heat transfer coefficient.

2.2 Numerical implementation and experiment

For the numerical experiments we have used the dimensions of the pilot unit (ACB GEC Alsthom, Nantes, France) that was used in [15]. Therefore, the 2D cylindrical domain has a radius of L = 0.09 m and a height of H = 0.654 m (see Figure 1).

We consider a representative example of sample food: a liquid type food with a small filling ratio. The dimensions and location of the sample is exactly the same as studied in [15] for solid type foods.

We present numerical tests computed in cylindrical coordinates using an iterative solver. We have considered the COMSOL Multiphysics 4.4 for solving the model. More precisely, velocity and pressure spatial discretization is based on P2–P1 Lagrange Finite Elements satisfying the Ladyzhenskaya, Babuska and Brezzi (LBB) stability condition. The convective diffusion equation is solved using a suitable direct method (UMFPACK: Unsymmetric MultiFrontal method for sparse linear systems) combined with a stabilization technique (GLS: Galerkin Least Squares, see [10,11,18]).

The physical parameters of the pressurizing medium are supposed to be equal to those of the water and depending on temperature and pressure. For the liquid food sample, water physical parameters are considered too. In this case, ρ, Cp and k parameters are computed through a shifting approach (see [12, 14]) from atmospheric pressure, and using a suitable linear interpolation for other values of pressure. For parameter α we use the expression described in [13]. Finally, dynamic viscosity η is obtained also by interpolation of data obtained using [9].

For general cases where the thermophysical properties of a particular food are not known, identification of these parameters making use of mathematical tools for inverse problems may be needed. For example, in [3] the authors discuss how to identify the heat transfer coefficient for a particular prototype. Identification of coefficients depending on temperature is considered, in a rigorous mathematical way in [2] for a general abstract case.

The environmental temperature, the reference temperature and the heat transfer coefficient used in the test are T_{amb} = 19.3 °C, T_{ref} = 40 °C and h = 28 $\text{W}\cdot\text{m}^{-2}\cdot\text{K}^{-1}$, respectively. Initial temperature in the sample is chosen equal to 22 °C. Thermophysical properties of the steel and the rubber cap of the sample holder were considered to be constant (ρ = 7833 $\text{kg}\cdot\text{m}^{-3}$, C_p = 465 $\text{J}\cdot\text{kg}^{-1}\cdot\text{K}^{-1}$) and k = 55 $\text{W}\cdot\text{m}^{-1}\cdot\text{K}^{-1}$ for steel and ρ = 1110 $\text{kg}\cdot\text{m}^{-3}$, C_p = 1884 $\text{J}\cdot\text{kg}^{-1}\cdot\text{K}^{-1}$ and k = 0.173 $\text{W}\cdot\text{m}^{-1}\cdot\text{K}^{-1}$ for rubber).

We have performed a particular numerical experiment simulating the

temperature evolution. For this sake, we consider a high pressure process as follows: for initial temperature

$$T_0 = \begin{cases} 40°\text{C in } \Omega_S, \\ 22°\text{C in } \Omega \backslash \Omega_S, \end{cases}$$

a constant pressure increase in the first 305 seconds until reaching 600 MPa is considered. Therefore, the derivative of pressure in the internal heat generation is

$$\frac{dP}{dt} = \begin{cases} \frac{600}{305}\, 10^6 \text{ Pa s}^{-1}, & 0 < t \leq 305, \\ 0 \text{ Pa s}^{-1}, & t > 305. \end{cases}$$

2.3 Numerical results

Figure 2 shows the temperature distribution under the considered high pressure process at time t = 15 min. Time–averaged temperature distribution for the considered case is represented in Figure 3. Both figures illustrate how the model captures the non-homogeneous temperature distribution in the domain. Figure 4 plots the evolution of the temperature at two points: the first one, B_1, is located at the center of the sample (at the symmetry axis) and the second one, B_2, at the surface of the sample, located at the same height than B_1 (see Figure 1). Evolution of sample mean temperature is also plotted. Therefore, the model and the numerical approximation of its solution are consistent with what is physically expected.

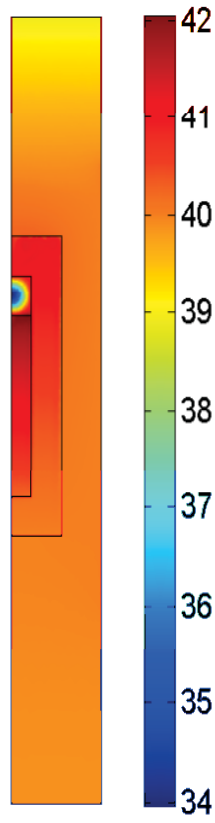

Figure 2. *Temperature distribution (°C) in the whole domain at t = 15 min after the considered proces.*

As already remarked in [15] for solid type foods, these results show that for liquid foods it can be also interesting to use an initial temperature for the food smaller than Tref in order to anticipate the temperature increase that results from compression, which allows to get a more uniform process avoiding big temperature gradients inside the food and temperatures much higher than T_{ref} (we remember that one of the goals of the high–pressure technology is to process the food without using high temperatures, which

degrade some of the main qualities of the food).

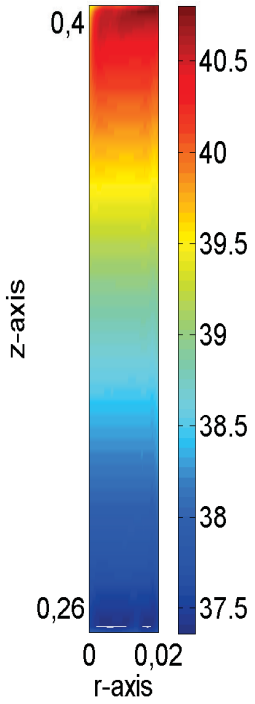

Figure 3. *Time–averaged temperature distribution (°C) during 15 min in the food sample after the considered process.*

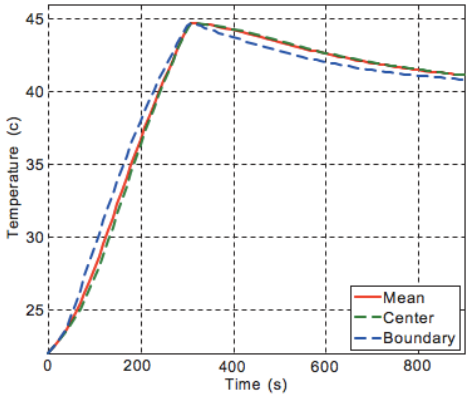

Figure 4. *Evolution of the sample's mean temperature (—), temperature in the center point B_1 (- -) and in the boundary point B_2 (- -) of the sample during the process.*

3. Optimization problem and future works

As remarked in previous Section 2.3, when the pressure is increased, the temperature of the food sample is also increased up to a point which may produces undesirable damages on the considered food sample (e.g., loss of organoleptic properties). Thus, proposing a treatment process that intends to increase the pressure up to a desired value by keeping the temperature lower than a prefixed threshold is of high interest. This objective can be reformulated by considering the following optimization problem:

$$\textit{minimize } |P(t)-P_{opt}| \textit{ such that } \textit{maximum}(T(x,y,t))<T_{opt}, \textit{ for any t in } (0,t_f) \textit{ and } (x,y) \textit{ in the food sample,}$$

where P_{opt} and T_{opt} are given.

To minimize this particular optimization problem, we could use, for instance, a global optimization algorithm such as the Controlled Random Search (CRS) [19,20]. CRS is a simple population based method that existed in Global Optimization literature before the hype of evolutionary algorithms. The basic algorithm is described in [21]. A more advanced variant due to Price is described in [22]. It generates more points in the convex hull of the population.

In future works, we propose to implement this optimization problem by using a Comsol Multiphysics with Matlab approach. Then, we will solve it with the CRS algorithm proposed in [6,7,19] and included in the free Matlab optimization package "Global

Optimization Platform", which can be downloaded at:
http://www.mat.ucm.es/momat/software.htm

4. Acknowledgements

We gratefully acknowledge the financial support of the Spanish "Ministry of Science and Innovation" under projects MTM2011-22658 and TIN2012-37483; the "Junta de Andalucía" and "European Regional Development Fund (ERDF)" through projects P10-TIC-6002, P11-TIC-7176 and P12-TIC301. Juana L. Redondo is a fellow of the Spanish "Ramón y Cajal" contract program, co-financed by the European Social Fund.

5. References

1. A. Delgado, C. Rauh, W. Kowalczyk and A. Baars, Review of modelling and simulation of high pressure treatment of materials of biological origin, Trends in Food Science & Technology 19(6), 329–336 (2008).
2. A. Fraguela, J.A. Infante, A.M. Ramos and J.M. Rey, Identification of a heat transfer coefficient when it is a function depending on temperature, WSEAS Trans. Math. 7(4), 160–172 (2008).
3. B. Guignon, A.M. Ramos, J.A. Infante, J.M. Díaz and P.D. Sanz, Determining thermal parameters in the cooling of a small-scale high pressure freezing vessel, International Journal of Refrigeration 29, 1152–1159 (2006).
4. R. Hayashi, Application of High Pressure to Food Processing and Preservation: Philosophy and Development. In Engineering and Food, vol. 2, Elsevier Applied Science, 815–826 (1989).
5. I. Indrawati, A.M. van Loey, C. Smout and M.E. Hendrickx, High hydrostatic pressure technology in food preservation. In Food preservation techniques, P. Zeuthen and L. Bogh-Sorensen Eds., Woodhead Publ. Ltd., Cambridge, 428–448 (2003).
6. B. Ivorra, B. Mohammadi, D.E. Santiago and J.G. Hertzog, Semi–deterministic and genetic algorithms for global optimization of microfluidic protein folding devices, International Journal of Numerical Method in Engineering 66(2), 319–333 (2006), doi:10.1002/nme.1562.
7. B. Ivorra, B. Mohammadi, A. M. Ramos, A multi-layer line search method to improve the initialization of optimization algorithms, European Journal of Operational Research (2015). DOI: http://dx.doi.org/10.1016/j.ejor.2015.06.044
8. W. Kowalczyk and A. Delgado, On convection phenomena during high pressure treatment of liquid media, High Pressure Research 27(1), 85–92 (2007).
9. E.W. Lemmon, M.O. McLinden and D.G. Friend, Thermophysical properties of fluid systems. In Linstron P.J. & Mallard W.G. (Eds.), NIST Chemistry Web Book. NIST Standard Reference Database, 69 (June 2005). National Institute of Standards and Technology. Gaitherburg MD, 20899 (http://webbook.nist.gov).
10. B. Mohammadi and O. Pironneau, Applied Shape Optimization for Fluids, Oxford University Press (2001).
11. B. Mohammadi, J. Santiago and J. Molho, Incomplete sensitivities in the design of minimal dispersion fluidic

channels, Comput. Methods Appl. Mech. Engrg. 192, 4131–4145 (2003).
12. T. Norton and D.W. Sun, Recent Advances in the Use of High Pressure as an Effective Processing Technique in the Food Indus- try, Food Bioprocess Technol 1, 2-34 (2008), doi:10.1007/s11947-007-0007-0
13. L. Otero, A.D. Molina–García and P.D. Sanz, Some interrelated thermophysical properties of liquid water and ice I. A user–friendly modeling review for food high–pressure processing, Critical Reviews in Food Science and Nutrition 42(4), 339–352 (2002).
14. L. Otero, A. Ousegui, B. Guignon, A. Le Bail and P.D. Sanz, Evaluation of the thermophysical properties of tylose gel un- der pressure in the phase change domain, Food Hydrocolloids 20, 449-460 (2006), doi:10.1016/j.foodhyd.2005.04.001.
15. L. Otero, A.M. Ramos, C. de Elvira and P.D. Sanz, A Model to Design High–Pressure Processes Towards an Uniform Temperature Distribution, J. Food Eng. 78, 1463–1470 (2007), doi:10.1016/j.jfoodeng.2006.01.020.
16. A.M. Ramos, R. Glowinski and J. Periaux, Pointwise control of the Burgers equation and related Nash equilibrium problems: computational approach, Journal of Optimization Theory and Applications 112(3), 499–516 (2002).
17. A. Tansakul and P. Chaisawang, Thermo-physical properties of coconut milk, Journal of Food Engineering 73(3), 273–280 (2006), doi:10.1016/j.jfoodeng.2005.01.035.
18. S. Turek, Efficient Solvers for Incom-pressible Flow Problems: An Algorithmic Approach in View of Computational Aspects. In LNCSE 6, Springer–Verlag (1999).
19. E.M. Hendrix, P.M. Ortigosa, I. García, On success rates for controlled random search. Journal of Global Optimization 21, 385-398 (2001).
20. E.M. Hendrix, B.G. Toth, Introduction to Nonlinear and Global Optimization. Springer, New York (2010).
21. P.M. Ortigosa, E.M.T. Hendrix, and J.L. Redondo. On heuristic bi-criterion methods for semi-obnoxious facility location. Computational Optimization and Applications. 2014. DOI: 10.1007/s10589-014-9709-1
22. W.L. Price, A controlled random search procedure for global optimization. The Computer Journal 20, 367-370 (1979).

Influence of Overhead Power Conductor Shape on its Temperature

J.C. del-Pino-López[1,*], D. Garrido-García[1], P. Cruz-Romero[1], A. Gómez-Expósito[1]

[1]Departamento de Ingeniería Eléctrica, Escuela Técnica Superior de Ingeniería, Universidad de Sevilla, Spain.
* Corresponding author: Camino de los descubrimientos s/n, 41092, Sevilla, vaisat@us.es

Abstract: This work deals with the design of new and more efficient overhead power conductors. To this purpose, a multiphysics finite elements model is developed in COMSOL Multiphysics©, where electromagnetic, thermal and fluid dynamics physics are fully coupled. By means of this model, different designs for the power conductors have been analyzed with the main goal of reducing its temperature when solar heating, radiation and forced convection heat transfer mechanisms are present, so that its current-carrying capacity may be increased in comparison to standard conductors. In addition, a parametric analysis has been carried out in order to analyze the influence of the main geometrical and environmental parameters on the temperature achieved in the conductor.

Keywords: overhead conductor, ampacity, temperature, forced convection, radiation.

1. Introduction

Due to the increase on electricity demand, the deregulation that imposes regulated revenues to transmission and distribution utilities, and the difficulty to build new overhead lines, in the last decades more and more power suppliers try to use power transmission lines up to their limits. This extreme use of power lines may lead to failures, so it is of interest to study more efficient designs of power lines with the main goal of obtaining power conductor with higher current-carrying capacity (ampacity). In this sense, overhead power conductors are affected by different heat transfer mechanisms: solar heating, radiation, conductive and forced convection heat transfer. The latter is the main heat evacuation mechanism, so it has much influence in the maximum temperature achieved by the power conductor. Additionally, the amount of heat evacuated by means of forced convection depends not only on the environmental conditions (wind direction, velocity and temperature), but also on the surface and shape of the conductor. Therefore, it is clear that a suitable shape for the conductor may increase the heat evacuated by forced convection, hence reducing its maximum temperature. As a consequence, its ampacity may be increased in comparison to standard designs. However, the problem to be solved is rather complex, since there are three physics involved: an electromagnetic problem coupled to thermal and fluid dynamics ones. In this situation, the best choice is the use of a multiphysics software like COMSOL

Multiphysics© for a suitable modelling of the system to be studied, in order to compute the temperature of the power conductor with accuracy.

The use of conductors of shape different from circle has been proposed previously, but not for the purpose of increasing the ampacity, but to reduce the wind load on the conductor.

2. Problem definition

The mathematical models to be solved, as well as the main hypotheses considered, are described in the following subsections.

2.1 Electromagnetic problem

The electromagnetic problem needs to be solved in order to compute the heat dissipated on the power conductor for a given current, which is the heat input for the thermal problem. This is performed based on the following assumptions:

1) The power conductor is straight and infinitely long, thereby rendering the problem 2D.
2) The phase current is sinusoidal with 50 Hz of frequency.
3) All materials have constant electrical properties, with the exception of conductive materials, whose electrical conductivity $\sigma(\theta)$ depends on temperature:

$$\sigma(\theta) = \frac{\sigma_0}{1+\alpha(\theta-20)}, \qquad (1)$$

where θ is the unknown temperature and σ_0 and α are the conductivity and the temperature coefficient of the material at 20 ºC, respectively.

4) Ferromagnetic materials are supposed to have constant permeability (μ).
5) Magnetics losses in ferromagnetic materials are neglected.

In this situation, the equation to be solved can be described as

$$\nabla \times \left(\frac{1}{\mu} \nabla \times \vec{A} \right) + j\omega\sigma\vec{A} = \vec{J}_e, \qquad (2)$$

where $\vec{A}$ is the magnetic vector potential, ω is the angular frequency and $\vec{J}_e$ the external current density. Once the problem is solved, the power losses generated in the conductor (Q_l) can be calculated from the total current density $\vec{J}$ as follows:

$$Q_l = \int \frac{\vec{J} \cdot \vec{J}^*}{\sigma} dS \qquad (3)$$

2.2 Thermal problem

The starting assumptions for the thermal problem are as follows:

1) Since the power cable is straight and infinitely long, the heat transfer problem can be formulated in 2D on the *x-y* plane.
2) All materials have constant thermal properties.
3) The air temperature is known (θ_{amb}).
4) Heat radiation (Q_{rad}) is present between the outer cable surface and the surrounding environment, with known surface emissivity (ε) of the materials.
5) Solar heating is present and it is considered as a known heat source input (Q_s).
6) Heat dissipation by forced convection is also considered (Q_{conv}).

7) Wind velocity is known and perpendicular to the power conductor, so that the system remains in 2D.

As a consequence, the temperature of the power conductor can be derived from the associated steady-state heat balance equation, expressed as

$$Q_l + Q_s = Q_{conv} + Q_{rad}, \quad (4)$$

where steady-state heat conduction inside the conductor is given by

$$\nabla \cdot (k \nabla \theta) + Q_l = 0, \quad (5)$$

the radiation heat loss is derived by

$$Q_{rad} = \varepsilon \cdot \sigma \cdot (\theta^4 - \theta_{amb}^4), \quad (6)$$

and the heat dissipated by forced convection is obtained from

$$\rho C_p u \cdot \nabla \theta = \nabla \cdot (k \nabla \theta), \quad (7)$$

where ρ is the air density, C_p the heat capacity of air, u the air velocity vector, θ is the unknown temperature, σ the Stefan-Boltzmann constant, and k the thermal conductivity of each material.

The coupled electromagnetic-thermal problem is iteratively solved as there are temperature-sensitive elements, such as the electrical conductivity of the conductor, which must be continuously corrected for the newly calculated temperature.

2.3 Fluid dynamics problem

As mentioned before, the air velocity field u around the conductor is required for the computation of the heat transferred by forced convection for a given wind velocity. This requires the computation of the continuity and momentum equations (Navier-Stokes equations) which govern the fluid flow, in the form of

$$\nabla \cdot (\rho u) = 0, \quad (8)$$

$$\rho u \cdot \nabla u = -\nabla p + \nabla \cdot \left(\mu \left(\nabla u + (\nabla u)^T \right) \right), \quad (9)$$

where p and μ are the air pressure and viscosity, respectively. In this case, air properties are temperature dependent also, and hence the fully coupled problem must be solved employing iterative techniques. In this sense, since wind velocity ranges from 1 m/s to 10 m/s, a k-ε turbulence model was considered.

3. Use of COMSOL Multiphysics©

The model developed for this study has implemented many features included in COMSOL. For example, the geometry of the power conductor has been simplified in order to parameterize its shape. In this sense, a conductor composed of aluminium (external layers) and steel (core) is modeled by means of two concentric circles, the external one made of aluminium and the internal one made of steel. Its shape is deformed in order to obtain different elliptical shapes. To this goal, a new parameter called Shape Factor (*SF*) is defined, which ranges from 0.5 to 1.5, being equal to 1 when a circular shape is desired. This is shown in Figure 1, where three different shapes are presented for three different values of this parameter. It will be employed later in the parametric analysis developed in next section. In order to keep the same cross section in the conductor for every *SF* value, the major (R_M) and minor radius (R_m) of the elliptic shapes are obtained as follows:

$$R_m = \frac{\sqrt{Area/\pi}}{SF}, \quad (10)$$

$$R_M = SF\sqrt{Area/\pi}, \quad (11)$$

where *Area* is the cross section of either aluminium or steel.

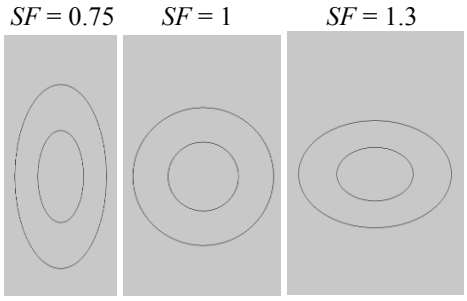

Figure 1. *Example of power conductor shapes for different SF values.*

On the other hand, four nodes are employed to define the multiphysics problem (Figure 2) with the following boundary conditions:

1) *Magnetic fields (mf):*
   - Linearized resistivity for the material of the power conductor by means of a second "Ampère's Law" node.
   - "Single-turn Coil" to impose the current flowing through the power conductor.
2) *Heat transfer (ht)*
   - "Heat transfer in solids" for the power conductor.
   - "Heat transfer in fluids" for the surrounding air.
   - "Temperature" and "Outflow" boundary conditions for the wind inlet and outlet boundaries.
   - "Heat source" in the power conductor, derived from the electromagnetic heating, as the heat input source for the thermal problem.
   - "Diffuse surface" in the external contour of the power cable to implement the heat losses due to radiation.
   - "Boundary Heat Source" to set the solar radiation Q_s as an additional heat source on the upper side of the conductor.
3) *Turbulent flow, k-ε (spf)*
   - "Inlet" to set the wind velocity in the external domain.
   - "Outlet" to set a pressure of 0 Pa in the outlet boundary.
   - "Symmetry" on the remaining boundaries.
4) *Multiphysics node*
   - "Non-isothermal Flow" node for coupling the thermal and fluid dynamic problems.
   - "Temperature Coupling" for coupling the thermal and the magnetic problems.

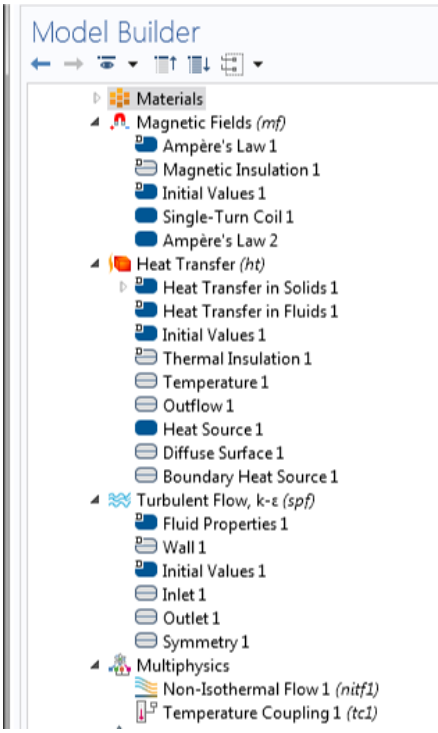

Figure 2. *Model nodes for the implementation of the multiphysics problem.*

In order to obtain accurate results, different operations have been applied to generate de mesh. In particular, 8 boundary layers are included in the external contour of the conductor, as shown in Figure 3, so that the velocity field can be accurately computed in the surrounding air.

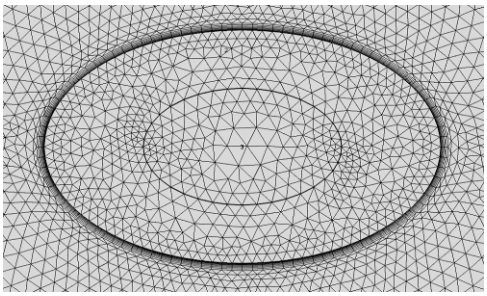

Figure 3. *Example of mesh for an elliptic power conductor.*

Eventually, a "Stationary" step is set on the "Study" node in order to compute the steady-state temperature of the system. In order to develop a parametric analysis, in several simulation it is also included a "Parametric sweep" node with the parameters to be analyzed.

4. Case study

The case of a 300 mm^2 power conductor is now analyzed. As mentioned previously, the stranded power cable is considered to be composed by two concentric circles (Figure 1 for SF = 1), taking the cross section of aluminum as twice of that of the steel. The properties of the materials are included in Table 1. Regarding boundary conditions, the temperature of air is taken as θ_{amb} = 20 ºC, for a wind velocity (V_{in}) ranging from 1 m/s to 10 m/s (wind blowing in the horizontal direction). Also, the heat input caused by solar radiation is taken as Q_s = 1200 W/m^2. Finally, the current through the conductor (I_0) will vary from 400 A to 1200 A.

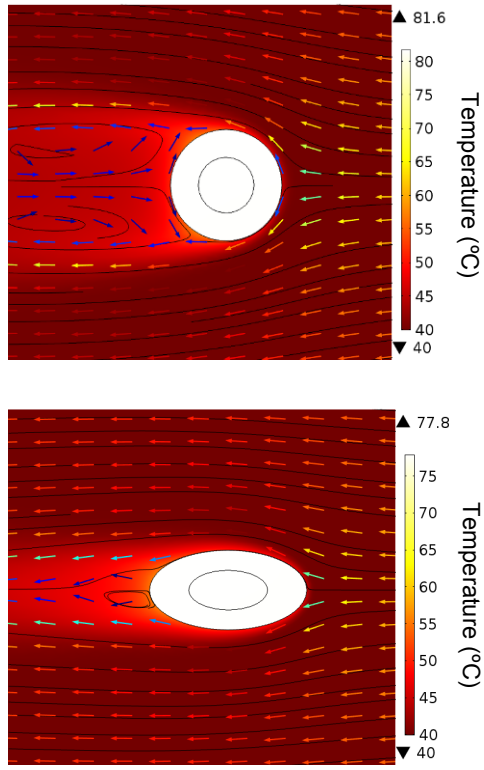

Figure 4. *Temperature and wind velocity field for SF = 1(up) and SF = 1.4 (down) (V_{in} = 1 m/s and I_0 = 750 A).*

Figure 4 shows an example of the temperature and velocity fields obtained for two values of SF. As can be observed, for the current flowing through the conductor (I_0 = 850 A), the use of an elliptical shape with SF = 1.4 leads to a reduction on its maximum temperature of about 4 ºC. As a consequence, it is of interest to study the effect of the geometrical shape of the power conductor on its temperature. In this sense, a parametric analysis is

developed next in order to analyze how the current carrying capacity (ampacity) of the power line can be improved.

Table 1: *Material properties*

Material	Property
Aluminium	$\sigma = 3.77 \cdot 10^7$ S/m $\alpha = 0.00403$ ºC^{-1} $\mu_r = 1$ $k = 240$ W/mK $\varepsilon = 0.8$
Steel	$\sigma = 4 \cdot 10^6$ S/m $\alpha = 0.005$ ºC^{-1} $\mu_r = 300$ $k = 56$ W/mK
Air	Properties from COMSOL library

4.1 Influence of SF and I_0

For a wind velocity of 1 m/s, Figure 5 shows the influence of *SF* and I_0 on the maximum temperature achieved in the power conductor. As can be observed, the temperature decreases with *SF* for a given current, being more interesting to use a power conductor with an elliptical shape with *SF* > 1. It is also observed that the difference in the maximum temperature for *SF* = 0.5 and *SF* = 1.5 is of about 10 ºC.

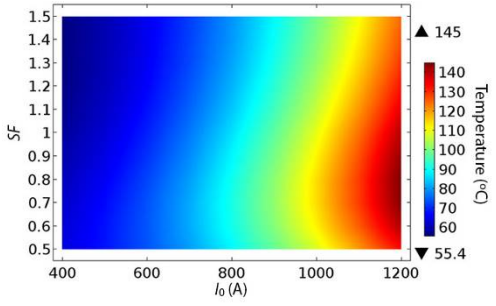

Figure 5. *Evolution of the maximum temperature with SF and I_0.*

As a consequence, the current-carrying capacity may be improved if a suitable *SF* is employed. For example, if the maximum temperature allowed by the power conductor is 90 ºC, then 825 A can flow through it for *SF* = 1, while for *SF* = 1.4 it can be increased up to 900 A, about 9 % higher for the values of θ_{amb} and V_{in} considered.

4.2 Influence of power conductor cross section

Another aspect to take into account is the size of the power conductor. In this sense, the following analysis is developed for conductor cross sections (S_c) from 300 mm^2 to 600 mm^2, considering a fixed current density flowing through the conductor of about 2.15 A/mm^2. In addition, wind velocity is of 1 m/s at 20 ºC. In this situation, Figure 6 shows the influence of the conductor cross section and its shape (*SF*) on its maximum temperature.

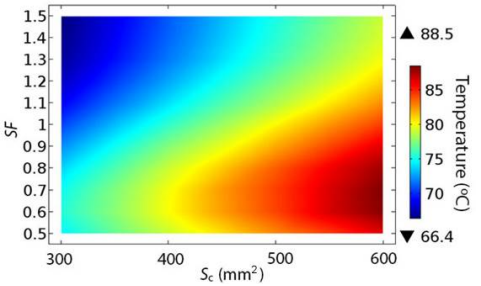

Figure 6. *Evolution of the maximum temperature with conductor cross section (S_c) and SF.*

From this figure it is derived that conductors with elliptical shape with *SF* > 1 are the best choice once again, since they achieve a lower temperature for a given cross section. In

this sense, for a given cross section, the improvement achieved on the temperature when changing from $SF = 1$ to $SF = 1.5$ is of about 5 ºC. However, for higher cross sections it is also observed a higher temperature due to the increase of the power losses.

4.3 Influence of wind velocity

In this case, for a current through the power conductor of about 1100 A, the evolution of the maximum temperature is shown in Figure 7. It is easily observed how a greater *SF* leads to lower temperatures, as concluded also in the previous sections, being more interesting the cases obtained with $SF > 1$ again.

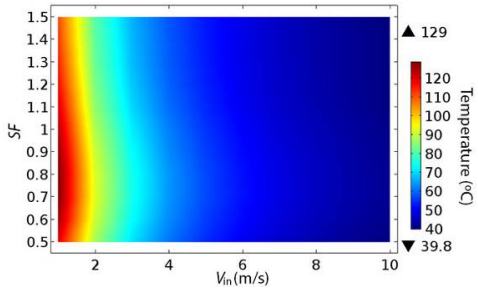

Figure 7. *Evolution of the maximum temperature with wind velocity and SF (I_0 = 1100 A and θ_{amb} = 20 ºC).*

Table 2: *Influence of wind velocity for θ_{amb} = 20 ºC*

		V_{in}		
		1 m/s	2 m/s	3 m/s
SF	1	123 ºC	88 ºC	71 ºC
	1.4	112 ºC	81 ºC	67 ºC
$\Delta\theta$		11 ºC	7 ºC	4 ºC

On the other hand, it is also concluded that, for any value of *SF*, the temperature decreases with wind velocity (as expected). However, it decreases more drastically in the range of 1 m/s to 3 m/s, while for higher velocity values its effect is less important. This is also represented in Table 2, where it is shown the difference ($\Delta\theta$) in the maximum temperature achieved by the power conductor for different wind velocities and *SF* values (for θ_{amb} = 20 ºC).

4.4 Influence of wind temperature

Another aspect to take into account is the air temperature θ_{amb}. If the air temperature is increased up to 40 ºC, results are different, as shown in Figure 8, where it can be observed how the maximum temperature is increased as expected.

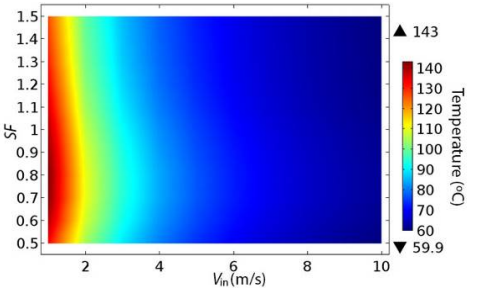

Figure 8. *Evolution of the maximum temperature with wind velocity and SF (I_0 = 1100 A and θ_{amb} = 40 ºC).*

In this situation, the heat evacuated by convection decreases due to a higher air temperature. Nonetheless, Figure 8 provides similar conclusions as those obtained in the previous section, since it is again observed how the reduction on the conductor's temperature is higher for

lower wind velocities, concluding that elliptical shapes are more efficient for low wind velocity conditions.

4.5 Influence of wind direction

In all the previous simulations, the direction in which the wind blows was considered parallel to the horizontal axis. But there may be situations where this is not true, since wind may have different angles of incidence in time. A situation like that is shown in Figure 9, where wind direction has an angle of incidence of about 30º.

It is clear that wind direction may influence on the maximum temperature achieved on the power conductor, and this is analyzed in Figure 10 for different values of *SF* and I_0 = 900 A. From this figure it is easily concluded once again that elliptical conductors with *SF* > 1 achieve lower temperature values for any wind direction.

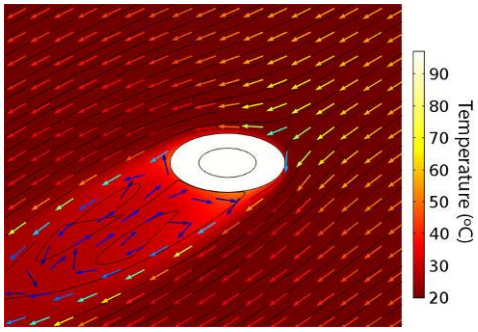

Figure 9. *Temperature and wind velocity field for SF = 1.4 and angle of incidence of 30º (V_{in} = 1 m/s, θ_{amb} = 20 ºC and I_0 = 900 A).*

However, it is also observed that the angle of incidence may affect negatively to the temperature of the power conductor if it changes from the horizontal wind direction case (angle of incidence of 0º). In particular, Figure 10 shows that, for *SF* > 1.2, the temperature of the power conductor may be increased in about 2 ºC when the angle of incidence changes from 0º to ±15º. Furthermore, if this angle reaches values in the order of 30º, the increase on the temperature is up to 7 ºC. Nonetheless, even in this unfavorable situation, the temperature in the elliptical conductor would be the same as the circular conductor at most.

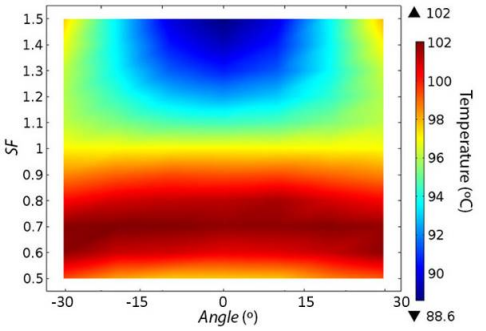

Figure 10. *Evolution of the maximum temperature with the angle of incidence and SF (θ_{amb} = 20 ºC).*

5. Conclusions

This work analyzes the influence of overhead power conductor's shape on its temperature when it is exposed to solar heating, radiation and forced convection. The complexity of the system requires the utilization of a powerful tool like COMSOL Multiphysics©. In this sense, a complete finite element model has been developed, where electromagnetic, thermal and fluid dynamics physics are fully coupled.

From this study it is concluded that overhead power conductors may increase their current carrying capacity if they have an elliptical shape instead

of a circular one. This increase may be in the range of 9% depending on the environmental conditions. In this sense, a parametric analysis has been also performed in order to show the influence of different geometrical and environmental parameters on the conductor's temperature. From this parametric analysis it is derived that the temperature of power conductors with elliptical shape is less sensitive to changes on the environmental conditions than the circular conductor, with the exception of the wind direction. This parameter influences negatively the temperature of the elliptical conductor, but this is only when it ranges from 0º to 30º. In the worst of these cases the temperature would achieve that of the circular conductor at most.

As a consequence of this study, future studies will be developed in order to check these results on actual stranded conductors as a preliminary step before experimental experiences.

6. References

1. T. Saito, Spiral-elliptic conductor with low-drag coefficient, *PES winter meeting*, 2000, Seattle.
2. CIGRÉ WG B2.43, Guide for Thermal Rating Calculation of Overhead Lines with high temperatures and real-time weather & load data, *Technical Report*, Draft 3.0 (2012).
3. L. Konti, A proposed algorithm for an overhead transmission line conductor temperature rise calculation, *International Transactions on Electrical Energy Systems*, **Volume 24**, page 578-596 (2014).
4. I. Makhkamova, *Numerical Investigations of the Thermal State of Overhead Lines and Underground Cables in Distribution Network*, Durham theses, Durham University (2011). Available at Durham E-Theses Online: http://etheses.dur.ac.uk/866/.
5. *COMSOL Multiphysics* Reference Manual, Version: October 2014 COMSOL 5.0.
6. *COMSOL* Heat Transfer Module User's Guide Version: October 2014 COMSOL 5.0.
7. *COMSOL* AC/DC Module User's Guide Version: October 2014 COMSOL 5.0.
8. *COMSOL* CFD Module User's Guide Version: October 2014 COMSOL 5.0.

7. Acknowledgements

This work has been supported by the Spanish Ministry of Science & Innovation under grant ENE2013-48428-C2-1-R.

Slag-Matte Decantation Studies

Cristian Bonţoiu[*1], Ignacio Moreno-Ventas Bravo[2], María Bacedoni, Felipe Jimenez Blas, Irene Ruiz Oria[3], Francisco Jimenéz[3], and Guillermo Rios Ransanz[3]

[1]University of Huelva, Department of Geology and [2]Applied Physics, [3]Atlantic Copper - Huelva, Spain.
* Corresponding author: cbontoiu@gmail.com

Abstract: Modelling the dynamics of copper slag-matte dropls has become an important issue of research with the advent of the new flash-smelter furnaces [1]. Better understanding of the thermal and chemical phenomena occurring at the interface between the two immiscible melts can improve the efficiency of the separation process. Preliminary studies of the decantation process of copper slag and matte are presented based on the Level Set method [2] implemented in Comsol. Ultimately, the drops shall be modelled as spheres released randomly in time with a statistical distribution of size, initial position and velocity. The current analysis focused on the degree of coalescence between the drops.

Keywords: copper, slag, matte, decantation**.**

1. Introduction

Modern production of copper takes place in flash furnaces like the one shown by Fig.1. Dry concentrate and oxygen-rich blast react in the reaction shaft.

For a chalcopyrite model the reactions are basically described by (1) and (2). They involve two immiscible melts corresponding to the dark solvus region showed in Fig. 2. The matte melt drops contain a high concentration of copper sulphur and metallic copper, and separate from the surrounding slag melt during a decantation process at the bottom of the furnace.

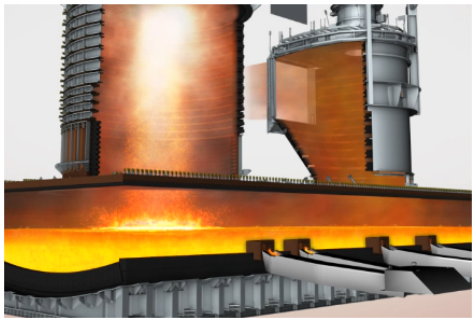

Figure 1**.** *Schematic view of a flash smelter furnace with the reaction shaft on the left, decantation bath on the bottom and outgas shaft on the right.*

$$2CuFeS_2(s) + 3.25O_2(g) \xrightarrow[\text{in oxygen enriched air}]{30\ ^\circ C} \underbrace{Cu_2S - 0.5FeS(l)}_{\text{molten matte}} + 1.5FeO(s) + 2.5SO_2(g) \quad (1)$$

$$2FeO(s) + SiO_2(s) \xrightarrow[\text{in quartz flux}]{1220\ ^\circ C,\ 30\ ^\circ C} \underbrace{Fe_2SiO_4(l)}_{\text{molten slag}}\ (1250\ ^\circ C) \quad (2)$$

The equilibrium composition of the two immiscible melts (slag and matte) is governed by the solvus curve shown in Fig. 2.

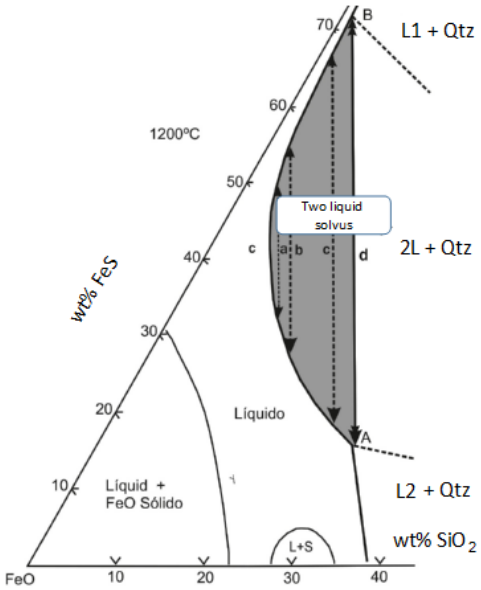

Figure 2. *Phase diagram for the system [SiO_2-FeO-FeS] modified from Yazawa and Kameda (1953) [3].*

All system compounds falling in the solvus region (dark area) are unmixed to the corresponding two liquids. Depending on their relative proportion there may be drops of one of them surrounded by the other. The four corresponding pair-lines (a, b, c, d) of the two immiscible liquids depend on the silica content of the system, reaching saturation along the d-line at the right side of the solvus region.

In the lower part of the reaction shaft and all over the settler melt drops are dragged by turbulent flow of the offgas before falling to the lighter slag melt bed. The size of these drops varies within the range of 1-50 µm. They enter into the slag bed with different momenta across all over the surface which separates the slag and offgas regions. Normally, melt drops are composed of small drops of matte surrounded by the slag melt. Matte drops are made of another immiscible system of two liquids, showing a chalcocite melt in the core region of the drop surrounded by metallic copper melt. The back-scattered electron microscope image seen in Fig. 3 shows one of these composite drops of matte melt surrounded by slag melt.

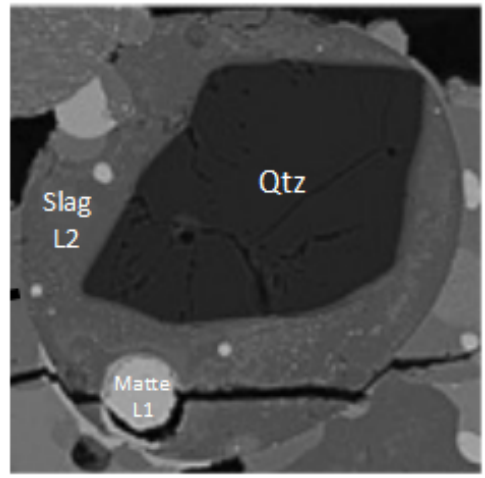

Figure 3. *Back-scattered electron image taken with an electron microscope, showing a composite melt drop from the reaction shaft dragged by chaotic flow of the offgas. The dark grain in the interior of the drop is one of the residual pieces of quartz from the flux.*

Decantation of the matte drops is eased by coalescence but at the same time it is marred by trapping in the slag bed. It is assumed that the finest drops remain caught in the slag layer while the larger make it through. As the slag melt is tapped from the settler through the tap holes, there is a residence time of the slag in the flash furnace, imposing a time for the decantation process. At the end, there is a range of the smallest drops that have no time for decantation. They are trapped in the slag layer and tapped out adding to the

overall mechanical losses balance of the copper smelting cycle. Coalescence of the matte drops is a concurrent process which has the opposite effect on the mechanical losses. The mechanics of the decantation process taking into account coalescence and dynamic effects further from a basic Stokes description is an important matter which needs complex numerical modelling using the tools of CFD. This article present preliminary findings of a the degree of decantation which occurs when a large number of matte drops fall through a layer of slag.

2. Model setup in Comsol

This section describes the 2D model built in the Comsol Multiphase Flow module in order to study the coalescence and decantation of drops. The closest model from Comsol gallery is the Rising Bubble one [4].

2.1 The Level Set Method

Because the system to be modelled consists of two immiscible liquids of large viscosity, the most suitable sub-module is Laminar Two-Phase Level Set. It uses an algorithm for the transient calculation of the interface function ϕ as:

$$\frac{\partial \phi}{\partial t} + \mathbf{u} \cdot \nabla \phi = \gamma \nabla \cdot \left(\varepsilon \nabla \phi - \phi(1-\phi) \frac{\nabla \phi}{|\nabla \phi|} \right) \quad (3)$$

where **u** [m/s] is the fluid velocity, while γ [m/s] and is a reinitialization parameter and ε [m] is the thickness of the interface between the two liquids. In practice setting up a decantation model implies defining the initial separation interfaces between the two fluids, setting up of the gravitation force and adding a zero- pressure point constraint for each interface to accelerate the numerical convergence. The most important parameters which control the dynamics of a many-drops system are the density ρ, dynamic viscosity μ, and surface tension σ.

For the particular case of slag and matte these values are shown in Table 1.

Parameter	Slag	Matte
ρ [kg/m^3]	3150	5100
μ [Pa·s]	0.45	0.04
σ [N/m]	0.17	

Table 1. *Material properties of slag and matte.*

2.2 Geometry Generation

The very first studies have been carried out with a small number of drops set up manually in order to understand basic dynamical effects.

```
public static double
 radGaussian(double radMean , double radStd)
{ double radius;
 Random r = new Random();
 radius = radMean + radStd*r.nextGaussian();
 return Math.abs(radius);}
int nosph = 0;
for(int i = 0; i < Nx; i++)
{ double xpos = Xmin + i*dX;
 for(int j = 0; j < Ny; j++)
 { nosph++;
  double ypos = Ymin + j*dY;
  String lab = "c";
  lab += Integer.toString(nosph);
  model.geom("geom1").create(lab, "Circle");
double rad = radGaussian(Ravg, Rstd);
model.geom("geom1").feature(lab)
     .set("r", Double.toString(rad));

model.geom("geom1").feature(lab)
     .set("pos", new String[]
     {Double.toString(xpos)
     ,Double.toString(ypos)});}}
```

Figure 4. *Java code used to generate drops with random diameter.*

For a large number of drops the initial geometry has been generated compiling a modified .java version of the Comsol model. A number of 225 drops with variable radius have been generated in a 2D grid through the code listed in Fig. 4.

3. Dynamical Effects

Dynamic effects generated by decantation can lead to the deformation of the drops depending on the value of the surface tension coefficient if the surface tension between them and the surrounding material is too small as it can be seen in Fig. 5.

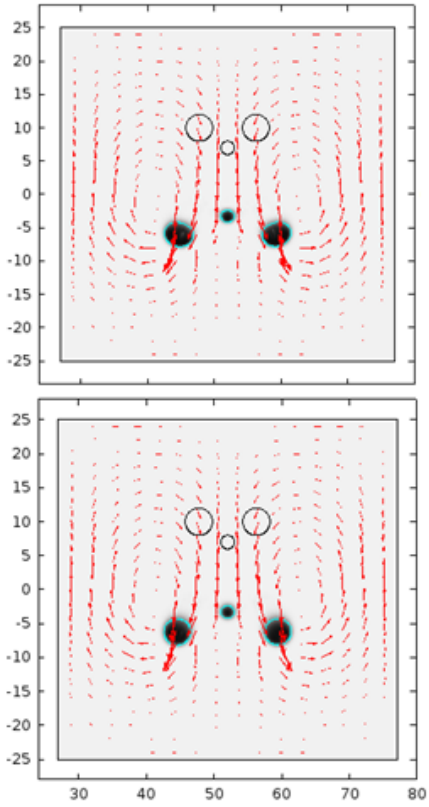

Figure 5. *Evolution of a three-drops system from the initial arrangement to a later time 0.5 s with a surface tension of 0.1 N/m (top) 0.5 N/m and (bottom).*

Consequently, motion of the continuous phase is driven to a certain magnitude and may act as a drag force on the other drops nearby, competing with gravity. Overall, this process makes the smallest size drops rise and avoid coalescence.

4. Coalescence

With a 2D distribution of drops generated as described in Sec. 2.2, time-dependent studies were carried out for a simulation time of a few seconds. As is can be seen from Fig. 6, there is a

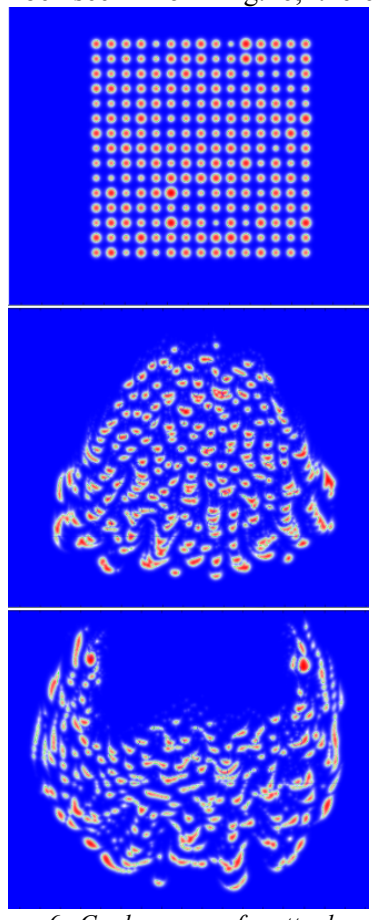

Figure 6. *Coalescence of matte drops (red) inside the slag layer (blue) within a time frame of 1 s.*

fast coalescence rate which accompanies the decantation process. This is due to the fact that the fall velocity is proportional with the mass of the drops given the dissipative motion in gravity.

Statistical representation of the drop radius shown in Fig. 7 reveals that the number of small size drops decreases in time and the initial Gaussian distribution develops a tail in the large size side.

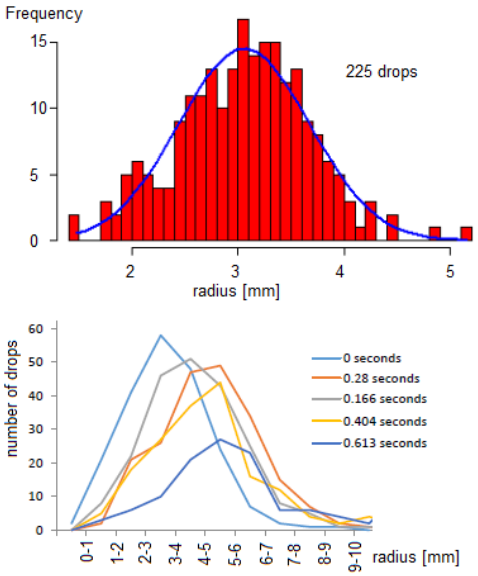

Figure 7. *Size distribution of drops at the beginning of the simulation (top) and during the coalescence process (bottom).*

These results confirm experimental findings reported for the frequency of matte drops size [5].

5. Conclusions

Numerically studied decantation reproduces the empirical pattern of size distribution for the matte drops trapped in slag. More complex studies are necessary to treat stability issues and enable 3D simulations. Two of the biggest challenges are:

- implementation of a moving mesh method to ensure consistency across the whole simulation domain;
- automatic computation of the drops size distribution at any time during the simulation.

Eventually, more realistic decantation studies, carried out with sub-millimeter drops will allow statistical estimates of the amount of the matte trapped in the slag layer, as a function of the initial starting conditions.

6. References

1. Schlesinger M., Extractive Metallurgy of Copper, Elsevier Science (2011)
2. Elin Olsson et al. A conservative level set method for two phase flow. Journal of Computational Physics, 210(1):225 – 246 (2005)
3. A. Yazawa, A. Kameda, Coper Smelting I. Partial liquidus diagram for FeS-FeO-SiO_2 system. Tech. Rep. Tohoku Univ. 16, 40-58 (1953)
4. https://www.comsol.es/model/rising-bubble-177
5. T. Loos, A. Lossin, Investigation of the silica slag of Norddeutsche Affinerie's Flash Furnace, Carlos Diaz Symposium on Pyrometallurgy, Toronto, Canada (2007).

7. Acknowledgements

The authors are grateful to Atlantic Copper S.L. (Huelva) for funding this research project.

Committees

Scientific committe

Ed Fontes. COMSOL AB, Sweden.

Ph.D. in Electrochemical Engineering from the Royal Institute of Technology in Stockholm. Ed Fontes is Chief Technology Officer at COMSOL. He is part of the group that decides the content and plans the work for developing COMSOL Multiphysics, its add on products, and COMSOL Sever. He is also deeply involved in the specification and implementation of the electrochemical engineering functionality in COMSOL.

José Manuel González Vida. University of Málaga.

Manager of the HySEA super-computation platform, at the Numerical Methods Laboratory at UMA. He is principal investigator in an international project with the NOAA Centre for Tsunami Research (U.S.A.), in which they apply numerical methods for tsunami simulations produced by submarine landslides.

Jesús Lucio García. University of Valladolid.

He is Physicist and PhD at University of Valladolid. He specialised in Electronics and has worked since then on many simulations, most of them with finite element software COMSOL Multiphysics (solar refrigeration by methanol adsorption on active charcoal, transitory study of a turbine, house heating and cooling by Trombe wall, aluminium melting by laser, and others). Main methods which he has worked with have been time series, neural networks and finite elements. Prof. Lucio has published several papers on international rated journals. He teaches Physics at University of Burgos since 1993.

Emilio Ruiz Reina. University of Málaga.

His research is mainly focused in the electrokinetics and rheology of concentrated nanoparticle suspensions and he successfully uses different numerical analysis methods. The collaboration with research groups and engineering companies in the field of finite element method simulations is among his regular activities, as well as teaching in specialized courses about COMSOL Multiphysics.

Benjamín Ivorra. Complutense University of Madrid.

PhD in Applied Mathematics at the University of Montpellier (France).His main research themes are about optimisation methods and their applications to industrial problems. In particular, he has extensively used COMSOL Multiphysics to model and solve design problems, such as improvement of microfluidic mixers, study of the effect of Pressure/Temperature in food treatment devices or conception of Pulsed Electric Field chambers.

Organizing committee

Emilio Ruiz Reina
Departamento de Física Aplicada II, Universidad de Málaga.
[+34] 95 195 22 91
eruizr@uma.es

Juan Antonio Rubio
Addlink Software Científico, S.L.
[+34] 93 415 49 04
jrubio@addlink.es